

Superconductivity in the two dimensional Hubbard Model

J. Beenen and D.M. Edwards

Department of Mathematics, Imperial College, London SW7 2BZ, UK

(24 february 1995)

Abstract

Quasiparticle bands of the two-dimensional Hubbard model are calculated using the Roth two-pole approximation to the one particle Green's function. Excellent agreement is obtained with recent Monte Carlo calculations, including an anomalous volume of the Fermi surface near half-filling, which can possibly be explained in terms of a breakdown of Fermi liquid theory. The calculated bands are very flat around the $(\pi, 0)$ points of the Brillouin zone in agreement with photoemission measurements of cuprate superconductors. With doping there is a shift in spectral weight from the upper band to the lower band. The Roth method is extended to deal with superconductivity within a four-pole approximation allowing electron-hole mixing. It is shown that triplet p -wave pairing never occurs. Singlet $d_{x^2-y^2}$ -wave pairing is strongly favoured and optimal doping occurs when the van Hove singularity, corresponding to the flat band part, lies at the Fermi level. Nearest neighbour antiferromagnetic correlations play an important role in flattening the bands near the Fermi level and in favouring superconductivity. However the mechanism for superconductivity is a local one, in contrast to spin fluctuation exchange models. For reasonable values of the hopping parameter the transition temperature T_c is in the range 10-100K. The optimum doping δ_c lies between 0.14 and 0.25, depending on the ratio U/t . The gap equation has a BCS-like form and $2\Delta_{max}/kT_c \simeq 4$.

71.10.+x, 71.27.+a, 74.20.Mn, 74.72.-h

I. INTRODUCTION

In 1957 Bardeen, Cooper and Schrieffer¹ provided, at a stroke, the essentials of a complete theory of the phenomenon of superconductivity as it was known then and for the next thirty years. However since the discovery of high temperature superconductivity in cuprate materials² it has been generally, although not universally, believed that a new mechanism is operating in these systems. It was established early on that one key element of the BCS mechanism, electron pairing, remains.³ However there is mounting evidence that the symmetry of the pairs is $d_{x^2-y^2}$ ⁴⁻⁸ rather than s -wave and this suggests an electronic mechanism for pairing rather than the original BCS phonon-mediated one.

The common element in all the cuprate superconductors is the CuO_2 plane in which the Cu atoms form a square lattice with an O atom at the midpoint of each pair of nearest-neighbour Cu atoms. In the simplest case of $La_2CuO_4 = (LaO)_2CuO_2$, with the assumption of La^{3+} and O^{2-} ions, the Cu charge is 2+ corresponding to a $3d^9$ configuration. In the presence of crystal field splitting one expects doubly occupied d_{xy} , d_{yz} , d_{zx} and $d_{3z^2-r^2}$ orbitals and a singly-occupied $d_{x^2-y^2}$ orbital. In the absence of interaction between the electrons the undoped system La_2CuO_4 would therefore be a metal whereas it is observed to be an antiferromagnetic insulator. This demonstrates the importance of strong repulsive Coulomb interaction on the Cu site which tends to localize the d electrons and produces a Mott insulator. In the doped system $La_{2-x}Sr_xCuO_4$, where La^{3+} ions are replaced by Sr^{2+} , the nominal occupation of the $x^2 - y^2$ Cu orbital is reduced to $1 - x$ and with $x \sim 0.15$ the system is metallic and superconducting with $T_c \sim 35K$.

Anderson⁹ was the first to propose that the essence of high temperature superconductivity is contained in the two dimensional (2D) square lattice Hubbard model¹⁰ with repulsive on-site interaction U . The atomic orbital in the model may be regarded as a Cu $d_{x^2-y^2}$ orbital hybridized with O p_x and p_y orbitals on neighbouring sites.^{11,12} In his recent work Anderson¹³ attributes the existence of superconductivity to electron transfer between CuO_2 planes. He proposes that electrons in the CuO_2 plane separate into uncharged spinons and charged holons, as they do in the one dimensional Hubbard model, where the electrons form a Luttinger liquid. This spin-charge separation inhibits the transfer of unpaired electrons between planes, but in Anderson's theory this constraint is removed upon pairing. The resultant decrease in total kinetic energy favours pairing and drives superconductivity. A difficulty with Anderson's theory is the absence of convincing evidence for spin-charge separation in two dimensions.

From the experimental point of view it is true that the critical temperature T_c tends to increase with the number of adjacent CuO_2 planes, although $Tl_2Ba_2CuO_6$ with rather isolated CuO_2 planes has $T_c = 85K$.¹⁴ Some interplanar interaction is presumably essential to stabilize superconductivity at finite T even when the primary mechanism, which sets the scale of the resultant T_c , operates within a plane. An analogous situation is a quasi-2D ferromagnet without magnetic anisotropy in which the scale of the Curie temperature is set by in-plane exchange interaction, although weak interplanar exchange is required to stabilize ferromagnetism at finite T .

An in-plane mechanism which is advocated by Pines and co-workers,¹⁵ Scalapino,¹⁶ and Moriya¹⁷ is based on electron pairing due to exchange of antiferromagnetic spin fluctuations. This type interaction leads inevitably to $d_{x^2-y^2}$ pairing and much of the experimental evi-

dence cited in its favour is evidence for $d_{x^2-y^2}$ pairing rather than for the spin fluctuation mechanism itself. In this paper we show how $d_{x^2-y^2}$ pairing arises in the 2D Hubbard model in a way which is not obviously related to antiferromagnetic spin fluctuations, although antiferromagnetic correlations between neighbouring sites are clearly present. The spin fluctuation mechanism has been strongly criticized by Anderson,¹⁸ who emphasizes the heuristic nature of Pines's model.

The published ab initio Monte Carlo calculations on the 2D Hubbard model have not produced any evidence of superconductivity.¹⁹ However for the small finite size systems considered the electron density cannot be varied continuously and it is possible that the favourable case of optimal doping is missed. Very recently Husslein *et al.*²⁰ have addressed this question by implementing projector Monte Carlo calculations for the 2D Hubbard model with nearest and next-nearest neighbour hopping parameters t, t' . This work was motivated by the 'van Hove scenario'²¹ in which, given a suitable interaction between electrons, a high T_c may emerge from the large density of states at the van Hove singularity associated with saddle-points in the band structure. To model a particular system t'/t is tuned so that for optimal doping, i.e. with a convenient electron density close to that with the highest observed T_c , the singularity occurs at the Fermi energy. In earlier work²¹ on the 'van Hove scenario' explicitly attractive electron interactions, such as the phonon mediated one, were considered and consequently the pairing was s -wave. The remarkable result of the new Monte Carlo calculations²⁰ is that $d_{x^2-y^2}$ pairing emerges in the repulsive U Hubbard model, but only when, for a given t'/t , the doping level is tuned to within $\pm 5\%$ of the optimum one. It is clear why superconductivity was missed in earlier Monte Carlo calculations. The new Monte Carlo results provide very satisfying confirmation of some of the results reported in this paper, which are obtained by a more analytical Green's function method. We will show how a combination of on-site electron repulsion and the band structure saddle-point leads to $d_{x^2-y^2}$ pairing and a fairly high T_c . Our approach gives a unified theory of quasiparticles in the normal and superconducting states. A slight surprise about the work of Husslein *et al.*²⁰ is that their modest interaction strength $U = 2t$ leads to sufficient correlation to give the effect.

We use a Green's function decoupling scheme originally due to Linderberg and Öhrn²² and first applied to calculations on the Hubbard model by Roth.²³ The formalism is reviewed in Sec. II and in Sec. III it is applied to the normal paramagnetic state of the 2D Hubbard model. It is shown that the Roth two-pole approximation gives excellent agreement with the quasiparticle dispersion curves found in recent Quantum Monte Carlo results by Bulut *et al.*²⁴. These authors have shown that their results are consistent with recent angular resolved photoemission measurements of the hole-doped cuprates. A natural extension of the method to superconductivity, now using a four-pole approximation, is made in Sec. IV. We find a superconducting state in which the gap is determined by a non-standard correlation function. In Sec. V a gap equation is derived in two ways, yielding a lower and upper bound to the gap. It is shown that triplet pairing cannot occur, but that singlet $d_{x^2-y^2}$ pairing is strongly favoured, with $T_c = 10 - 100\text{K}$. The critical temperature T_c is strongly dependent on doping, with the optimum doping corresponding to the case where the saddle-point of the band structure is situated exactly at the Fermi level. This links our work to the 'van Hove scenario', although none of its ideas were imposed beforehand, unlike work by other authors.²⁵ Our results arise from the Hubbard model and the decoupling scheme only.

II. THE FORMALISM

In this paper we wish to determine Green's functions of the Hubbard model¹⁰ with hamiltonian

$$\hat{H} = t \sum_{\langle i,j \rangle} \sum_{\sigma} c_{i\sigma}^{\dagger} c_{j\sigma} + U \sum_i n_{i\sigma} n_{i-\sigma} - \mu \sum_{i,\sigma} n_{i\sigma}, \quad (2.1)$$

including the chemical potential in a standard notation. The equation of motion for a retarded Green's function $\langle\langle \hat{A}; \hat{B} \rangle\rangle$ takes the form

$$\omega \langle\langle \hat{A}; \hat{B} \rangle\rangle = \langle [\hat{A}, \hat{B}]_+ \rangle + \langle\langle [\hat{A}, \hat{H}]; \hat{B} \rangle\rangle, \quad (2.2)$$

where $\langle \dots \rangle$ denotes the thermal average. Note the introduction of a new Green's function $\langle\langle [\hat{A}, \hat{H}]; \hat{B} \rangle\rangle$, which implies that an infinite set of equations needs to be solved. A very satisfying way to decouple this set of equations is to introduce a set of operators $\{\hat{A}_n\}$, which are believed to be the most relevant to describe the one particle excitations of the system of interest. Formally this assumption is that

$$[\hat{A}_n, \hat{H}] = \sum_m K_{nm} \hat{A}_m. \quad (2.3)$$

Here, for the application of the formalism on the 2D Hubbard model in the thermodynamic limit for several parameter ratio's U/t , we follow Roth²³ in choosing two operators of Bloch type

$$\hat{A}_{1\vec{k}\sigma} = c_{\vec{k}\sigma} = \frac{1}{\sqrt{L}} \sum_i e^{i\vec{k} \cdot \vec{R}_i} c_{i\sigma}, \quad (2.4)$$

$$\hat{A}_{2\vec{k}\sigma} = d_{\vec{k}\sigma} = \frac{1}{\sqrt{L}} \sum_i e^{i\vec{k} \cdot \vec{R}_i} n_{i-\sigma} c_{i\sigma} \quad (2.5)$$

to describe the normal, spatially uniform, state of the system. Here L is the number of lattice sites in the system. The restriction to spatial uniformity allows discussion of ferromagnetic states,^{23,26} but additional operators are necessary to describe antiferromagnetic states.^{27,28} To describe superconducting states, we shall also introduce additional 'hole' operators to supplement the 'electron' operators (2.4),(2.5):

$$\hat{A}_{3\vec{k}\sigma} = c_{-\vec{k}-\sigma}^{\dagger} = \frac{1}{\sqrt{L}} \sum_i e^{i\vec{k} \cdot \vec{R}_i} c_{i-\sigma}^{\dagger}, \quad (2.6)$$

$$\hat{A}_{4\vec{k}\sigma} = d_{-\vec{k}-\sigma}^{\dagger} = \frac{1}{\sqrt{L}} \sum_i e^{i\vec{k} \cdot \vec{R}_i} n_{i\sigma} c_{i-\sigma}^{\dagger}. \quad (2.7)$$

The coefficients K_{nm} in Eq. (2.3) are determined by anticommuting both sides of Eq. (2.3) with each element of the operator set $\{\hat{A}_n\}$ and then taking the thermal average. This can be written in matrix notation as

$$\mathbf{E} = \mathbf{K}\mathbf{N}, \quad (2.8)$$

where the energy and normalization matrices, \mathbf{E} and \mathbf{N} , are given by

$$E_{nm} = \left\langle \left[[\hat{A}_n, \hat{H}], \hat{A}_m^\dagger \right]_+ \right\rangle, \quad (2.9)$$

$$N_{nm} = \left\langle [\hat{A}_n, \hat{A}_m^\dagger]_+ \right\rangle. \quad (2.10)$$

Combining Eqs. (2.2), (2.3), and (2.8)- (2.10) we obtain

$$\left\langle \langle \hat{A}_n; \hat{B} \rangle \right\rangle = \sum_m \tilde{G}_{nm} \left\langle [\hat{A}_m, \hat{B}]_+ \right\rangle, \quad (2.11)$$

where $\tilde{\mathbf{G}}$ is given by

$$\tilde{\mathbf{G}} = \mathbf{N}(\omega\mathbf{N} - \mathbf{E})^{-1}. \quad (2.12)$$

If $\hat{B} = \hat{A}_m^\dagger$ we obtain for the Green's function matrix, whose elements are given by

$$G_{nm}(\omega) = \left\langle \langle \hat{A}_n; \hat{A}_m^\dagger \rangle \right\rangle, \quad (2.13)$$

a solution in terms of the matrices \mathbf{E} and \mathbf{N} :

$$\mathbf{G}(\omega) = \mathbf{N}(\omega\mathbf{N} - \mathbf{E})^{-1}\mathbf{N}. \quad (2.14)$$

This decoupling procedure was first proposed by Linderberg and Öhrn.²² Soon after Roth²³ applied this procedure to study ferromagnetism in the 3D infinite U Hubbard model in the thermodynamic limit. It can be shown that the formalism is essentially equivalent to the Mori-Zwanzig projection technique²⁹⁻³¹ and strongly related to moment methods^{32,33} based on the assumption that the spectral function is a finite sum of weighted delta functions.^{34,35}

The matrix elements E_{nm} and N_{nm} involve correlation functions which should be determined self-consistently from the calculated Green's functions as far as possible. Sometimes however, as discussed in Sec. III, one must introduce further Green's functions. The standard relationship between correlation function and Green's function may be written as

$$\langle \hat{B}\hat{A} \rangle = \frac{1}{2\pi i} \oint f(\omega) \left\langle \langle \hat{A}; \hat{B} \rangle \right\rangle_\omega d\omega, \quad (2.15)$$

where $f(\omega)$ is the Fermi function $f(\omega) = (e^{\beta\omega} + 1)^{-1}$ and the contour encircles the real axis without enclosing any poles of $f(\omega)$. The chemical potential μ is determined by the condition

$$n = L^{-1} \sum_{\vec{k}} \langle c_{\vec{k}\sigma}^\dagger c_{\vec{k}\sigma} \rangle = \frac{1}{2\pi i L} \sum_{\vec{k}} \oint f(\omega) G_{11\vec{k}}(\omega) d\omega, \quad (2.16)$$

where $n = \langle n_{i\sigma} \rangle$ is the average site occupation per spin.

III. THE NORMAL STATE

For the normal paramagnetic state of the Hubbard model, within the 2-operator set $\{\hat{A}_{1\vec{k}\sigma}, \hat{A}_{2\vec{k}\sigma}\}$, the energy and normalization matrices \mathbf{E}_2 , \mathbf{N}_2 are given by²³

$$\mathbf{E}_2 = \begin{bmatrix} \epsilon_{\vec{k}} + Un - \mu & (\epsilon_{\vec{k}} - \mu + U)n \\ (\epsilon_{\vec{k}} - \mu + U)n & (U - \mu)n + \epsilon_{\vec{k}}n^2 + n(1 - n)W_{\vec{k}} \end{bmatrix} \quad (3.1)$$

$$\mathbf{N}_2 = \begin{bmatrix} 1 & n \\ n & n \end{bmatrix}. \quad (3.2)$$

The Green's function matrix is readily found using Eq. (2.14). Here $\epsilon_{\vec{k}}$ is the unperturbed band energy

$$\epsilon_{\vec{k}} = t \sum_{\langle j \rangle_i} e^{i\vec{k} \cdot (\vec{R}_j - \vec{R}_i)} \quad (3.3)$$

and $W_{\vec{k}}$ may be written as:

$$n(1 - n)W_{\vec{k}} = w_0 + w_1\epsilon_{\vec{k}}, \quad (3.4)$$

with

$$w_0 = - \sum_{\langle j \rangle_i} t \langle c_{i\sigma}^\dagger c_{j\sigma} (1 - n_{i-\sigma} - n_{j-\sigma}) \rangle, \quad (3.5)$$

$$w_1 = \frac{1}{4} (\langle N_j N_i \rangle - \langle N_j \rangle \langle N_i \rangle) + \langle \vec{S}_j \cdot \vec{S}_i \rangle - \langle c_{j\sigma}^\dagger c_{j-\sigma}^\dagger c_{i-\sigma} c_{i\sigma} \rangle. \quad (3.6)$$

Here $N_j = n_{j\sigma} + n_{j-\sigma}$ and \vec{S}_j are the total number operator and the spin operator respectively for site j . Sites j and i are nearest neighbours as indicated by the j summation $\langle j \rangle_i$ in Eqs. (3.3) and (3.5). For the 2D Hubbard model on a square lattice the unperturbed band energy is given by

$$\epsilon_{\vec{k}} = 2t (\cos k_x a + \cos k_y a) \quad (3.7)$$

with a the lattice constant. To model the CuO_2 plane we take $t < 0$ so that the bottom of the band is at the Γ -point $k_x = k_y = 0$. The occupation number n and the correlation functions in w_0 may be calculated from Green's functions G_{11} and G_{12} by means of Eq. (2.15). The correlation functions in w_1 cannot be determined directly in this way. A natural way to determine the density and spin correlation functions in w_1 would be to extend the formalism to deal consistently with the corresponding two-particle Green's functions. This would have the advantage of yielding the spin dynamics of the system and work along these lines is in progress. Here, however, we follow Roth's original procedure and introduce extra operators \hat{B}_i . Correlations of the form $\langle \hat{A}_1 \hat{B}_i \rangle$ can then be calculated within the decoupling (2.3) by using Eqs. (2.11) and (2.15). The details are given in Roth's paper.²³

Thus to investigate the normal state of the 2D Hubbard model we follow precisely the method Roth²³ originally applied to the three dimensional cubic lattice. The use of two operators, \hat{A}_1 and \hat{A}_2 corresponds to a two-pole approximation to the Green's function. The resulting Green's function therefore consists of two terms, each corresponding to a quasiparticle band:

$$G_{1\vec{k}}(\omega) = \frac{\alpha_{1\vec{k}}}{\omega - \xi_{1\vec{k}}} + \frac{\alpha_{2\vec{k}}}{\omega - \xi_{2\vec{k}}} \quad (3.8)$$

with

$$\alpha_{1\vec{k}} = \frac{1}{2} + \frac{U(1 - 2n) - \epsilon_{\vec{k}} + W_{\vec{k}}}{2X_{\vec{k}}} \quad ; \quad \alpha_{2\vec{k}} = 1 - \alpha_{1\vec{k}}, \quad (3.9)$$

$$\xi_{1\vec{k}} = \frac{U + \epsilon_{\vec{k}} + W_{\vec{k}} - 2\mu}{2} - \frac{X_{\vec{k}}}{2} \quad ; \quad \xi_{2\vec{k}} = \xi_{1\vec{k}} + X_{\vec{k}}, \quad (3.10)$$

and

$$X_{\vec{k}} = \sqrt{(U - \epsilon_{\vec{k}} + W_{\vec{k}})^2 + 4nU(\epsilon_{\vec{k}} - W_{\vec{k}})}. \quad (3.11)$$

It has been shown that this Green's function conserves the first four moments of the spectral density.³⁵ The quasiparticle bands $\omega = \xi_{1\vec{k}}$ and $\omega = \xi_{2\vec{k}}$ satisfy $\det(\omega \mathbf{N}_2 - \mathbf{E}_2) = 0$. They are plotted in Fig. 1, for $U = 8|t|$ and different site occupations $\langle N \rangle = 2n$, along symmetry lines in the two dimensional Brillouin zone. The quasiparticle energies are relative to the chemical potential μ and comparison is made with the non-interacting band $\epsilon_{\vec{k}}$, relative to the non-interacting chemical potential, and with very recent Quantum Monte Carlo results by Bulut *et al.*²⁴. The agreement with the Monte Carlo results is remarkable and this is a strong indication that the Roth two-pole approximation represents the Green's function rather well. This is reasonable since the spectral functions of Bulut *et al.*²⁴ are dominated by two peaks which define the quasiparticle energies for each \vec{k} . Near $\vec{k} = (\pi, \pi)$ there is also an additional broad bump at lower energy, but its weight is very small. One striking feature is the flattening at the top of the lower band around $\vec{k} = (\pi, \pi)$, extending to the saddle-point at $\vec{k} = (\pi, 0)$ and halfway to $\vec{k} = (0, 0)$. Very flat bands have also been observed near the $(\pi, 0)$ point in recent angular resolved photoemission (ARPES) experiments on hole doped cuprate superconductors such as $Bi_2Sr_2CaCu_2O_{8+\delta}$ (Bi 2212),³⁶ $Bi_2Sr_2CuO_6$ (Bi2201),³⁷ $YBa_2Cu_4O_8$ (YBCO 124),^{38,39} and $YBa_2Cu_3O_7$ (YBCO 123).^{38,40} It is clear from our calculations that this feature is associated to a large extent with nearest neighbour antiferromagnetic correlations $\langle \vec{S}_i \cdot \vec{S}_j \rangle < 0$. Because $\langle \vec{S}_i \cdot \vec{S}_j \rangle$ is by far the most important contributor to w_1 for the occupations shown, w_1 will be negative, so that $W_{\vec{k}}$ decreases with increasing $\epsilon_{\vec{k}}$. This leads to a narrowing and, near the top, a flattening of the lower band. $\langle \vec{S}_i \cdot \vec{S}_j \rangle$ increases with occupation, so the effect is pronounced when approaching half-filling. The flattening near the top is also responsible for a clear gap between the upper and lower band, even for U no larger than the unperturbed bandwidth. The densities of states calculated from the one-particle Green's function are shown in Fig. 2.

One feature that the Quantum Monte Carlo results appears to share with our results is an anomalous Fermi surface volume for $\langle N \rangle \gtrsim 0.8$. In Fig. 3 we plot the Fermi surfaces associated with our calculated bands and the non-interacting bands of Fig. 1. It is clear that the volume, or area in two dimensions, of the calculated Fermi surface is always larger than the non-interacting one. Since the Quantum Monte Carlo bands agree well with ours along symmetry lines, the corresponding Fermi surfaces may be expected to be similar. Certainly for $\langle N \rangle = 0.94$ it seems that the Quantum Monte Carlo data are definitely incompatible with a Fermi surface of normal volume. However, according to Luttinger's theorem⁴¹ the volume enclosed by the Fermi surface of an interacting Fermi liquid is equal to that of the non-interacting system. We would not want to conclude that there is a breakdown of Fermi liquid theory on the basis of our own calculations, because, as will be discussed below, the two-pole approximation will always lead to a Fermi surface enclosing an enlarged volume when only the lower band is occupied. But the Monte Carlo method in principle yields exact results for the model, so the apparent anomalous Fermi surface volume must be taken seriously. It must be remembered however that the Quantum Monte Carlo calculations²⁴ were executed at a finite temperature, $T = 0.5|t|$ in this case. A possibility is that the enlarged Fermi surface volume is a temperature effect and that the volume shrinks to its normal volume as $T \rightarrow 0$, although this means that the form of the Fermi surface and the bands would change considerably in the process. In order that the chemical potential moves in the right direction with increasing temperature, the Fermi level at $T = 0$ would have to lie above the van Hove singularity where the density of states has a negative gradient. Thus electron interaction would have produced a strong distortion of the Fermi surface which, although conserving the enclosed volume, changes the topology. Another explanation might be that a transition from a Fermi liquid to a non-Fermi liquid, of the type predicted by Edwards and Hertz,⁴² is occurring as $\langle N \rangle$ increases through a critical value N_c . In the Edwards-Hertz theory, based on a modified Hubbard alloy analogy, a $T = 0$ phase transition occurs at a value of $N_c < 1$ when U is larger than the bandwidth. For $\langle N \rangle < N_c$ we have a normal Fermi liquid with a Fermi surface of normal volume defined by a finite Migdal discontinuity associated with quasiparticles of infinite lifetime. For $\langle N \rangle > N_c$ there is no Migdal discontinuity since all quasiparticles have a finite lifetime, attributed by Edwards and Hertz to very strong spin disorder scattering. However clear quasiparticle peaks in the spectral functions still exist, just as in the Monte Carlo data, and the points in \vec{k} space where they cross the chemical potential define a 'Fermi surface'. It is found⁴³ that for $\langle N \rangle > N_c$ the volume of this Fermi surface is enlarged compared with the non-interacting one and spectral functions and quasiparticle bands have been calculated for the 2D Hubbard model within the Edwards-Hertz approach so that a detailed comparison with the Monte Carlo data can be made. It is clear on general grounds that, if the 'Fermi surface' volume is indeed anomalous, one would not expect a Migdal discontinuity with sharp quasiparticles because this is a vestige of the non-interacting situation and would only occur at a surface of normal volume.

We now return to the present Roth approach which cannot describe a sharp transition at a critical N_c but which gives a smooth crossover from Fermi surfaces of almost normal volume at smaller $\langle N \rangle$ to enlarged surfaces at $\langle N \rangle$ closer to 1. The major defect of the two-hole approximation is that the quasiparticles, whose energies appear to be given rather accurately, are not subject to any lifetime broadening. The origin of the enlarged Fermi

surface within this approximation is seen most clearly in the limit of very large U where the effect is most pronounced. For $U \rightarrow \infty$ the one-electron Green's function G_{11} is easily found from Eqs. (3.8)-(3.11) to take the form

$$G_{11} \simeq \frac{1-n}{\omega - (1-n)\epsilon_{\vec{k}} - nW_{\vec{k}} + \mu} + \frac{n}{\omega - n\epsilon_{\vec{k}} - (1-n)W_{\vec{k}} - U + \mu}. \quad (3.12)$$

For $\langle N \rangle = 2n < 1$ only the lower band, associated with the pole of the first term, is occupied. Since each state in this band has weight $1-n$, whereas for a non-interacting case each state has weight 1, the Fermi surface volume is increased relative to the non-interacting one by a factor $(1-n)^{-1}$. For example if $\langle N \rangle = \frac{2}{3}$, the enlargement factor is $\frac{3}{2}$ and the Fermi surface volume corresponds to a half-filled ($\langle N \rangle = 1$) non-interacting situation. Since $W_{\vec{k}}$ depends on \vec{k} only through $\epsilon_{\vec{k}}$, as is seen from Eq. (3.4), it follows from Eq. (3.10) that a quasiparticle constant energy surface enclosing a given volume coincides with the non-interacting energy surface enclosing the same volume. Thus, with $U \rightarrow \infty$, for $\langle N \rangle = \frac{2}{3}$ we have the square Fermi surface $\epsilon_{\vec{k}} = 0$, but for finite U , with a less pronounced enlargement factor, the square Fermi surface occurs for larger $\langle N \rangle$. The square Fermi surface plays an important role in the superconducting state described in the following sections because, for given U , optimum doping (highest T_c) occurs with the occupation $\langle N \rangle$ corresponding to the square Fermi surface. This corresponds to having a van Hove singularity at the Fermi level for some finite doping and we have argued above that this must be the case at $T = 0$ to be consistent with the high temperature Monte Carlo data. Thus even if the anomalous Fermi surface volume of the Roth method is spurious we believe the topology of the Fermi surface is described quite well.

We wish to emphasize again the remarkable agreement shown in Fig.1 between the quasiparticle bands calculated by the Roth two-pole approximation, using precisely her method of evaluating various correlation functions which occur, and those given by the Monte Carlo calculations of Bulut *et al.*²⁴. Our calculations agree with the Monte Carlo data not only for the location of the bands, but also for the spectral weight distribution over the two bands. This is shown in Fig. 4 where we show, for several points along the $k_x = k_y$ line in the Brillouin zone, our two delta functions with weights $\alpha_{1\vec{k}}$ and $\alpha_{2\vec{k}}$. These weights compare well with the areas under the peaks of the spectral functions found by Bulut *et al.*²⁴ While the spectral weight distribution is dispersionless for $U \rightarrow \infty$, for intermediate U ($U = 8|t|$) we find a strong dispersion. We also find that there is a strong weight transfer upon doping from the upper band $\omega = \xi_{2\vec{k}}$ to the lower band $\omega = \xi_{1\vec{k}}$, as shown in Fig. 5. This weight transfer is particularly strong around the (π, π) point for intermediate U . A strong weight transfer from high energy scale to low energy scale upon doping has been observed in electron loss experiments⁴⁴ and optical spectroscopy experiments⁴⁵ on high temperature cuprate superconductors. Applying strong-coupling perturbation theory, Eskes *et al.*⁴⁶ find a similar weight transfer.

We may mention here that the Roth procedure, again followed precisely, also gives a good description of the occurrence of ferromagnetism in the 2D Hubbard model. The ferromagnetic region of the $(\langle N \rangle, t/U)$ plane is found to be²⁶ somewhat larger than the best variational estimates,⁴⁸ but the result is again remarkably good considering the subtlety of the energy

balance in this problem and the simplicity of the method. This contrasts strongly with the Hubbard I approach,¹⁰ which corresponds to setting $W_{\vec{k}} = 0$. Roth²³ pointed out that the constant shift w_0 in $W_{\vec{k}}$ [see Eq. (3.4)] for the minority spin band is essential to stabilize the state of complete spin alignment for large U near half-filling. Recently Hewson and Wasserman⁴⁷ showed how an approach equivalent to the Roth one leads to the results of slave-boson mean field theory in the Anderson impurity model; here again the shift in the impurity arising from w_0 is essential to place the resonant state correctly near the Fermi level. These successes of the present approach encourage us to consider another subtle problem, superconductivity, in the next section. We shall see that an anomalous correlation function which characterizes the superconducting state is generated automatically, just like the correlation functions in $W_{\vec{k}}$.

IV. THE SUPERCONDUCTING STATE

To discuss superconductivity we need to mix electron and hole operators and evaluate anomalous correlation functions in which particle number is not conserved. In this context we note that the procedure described in Sec. II, applied on the BCS reduced Hamiltonian and using the operator set $\{c_{\vec{k}\sigma}, c_{-\vec{k}-\sigma}^\dagger\}$ yields the whole BCS formalism¹ in Nambu-Gor'kov form.⁴⁹ As indicated in Sec. II, for the Hubbard model we use the four operators (2.4)-(2.7) and hence obtain a four-pole approximation to the Green's functions. The 4x4 energy and normalization matrices \mathbf{E}_4 and \mathbf{N}_4 may each be partitioned into four 2x2 matrices. The upper left 2x2 matrices are just \mathbf{E}_2 and \mathbf{N}_2 , given by Eqs. (3.1) and (3.2), and the lower right 2x2 matrices are easily shown to be $-\mathbf{E}_2$ and $+\mathbf{N}_2$. The elements of the off-diagonal blocks involve anomalous correlation functions and are as follows:

$$N_{13} = N_{24} = N_{31} = N_{42} = 0, \quad (4.1)$$

$$N_{14} = -N_{23} = N_{41}^* = -N_{32}^* = \langle c_{i\sigma} c_{i-\sigma} \rangle, \quad (4.2)$$

$$E_{13} = E_{31}^* = U \langle c_{i-\sigma} c_{i\sigma} \rangle, \quad (4.3)$$

$$E_{14} = E_{32}^* = (\epsilon_{\vec{k}} - \mu) \langle c_{i\sigma} c_{i-\sigma} \rangle, \quad (4.4)$$

$$\begin{aligned} E_{23} = E_{41}^* &= (U - \epsilon_{\vec{k}} - \mu) \langle c_{i-\sigma} c_{i\sigma} \rangle \\ &+ \sum_{\langle l \rangle_i} t \langle c_{i-\sigma} c_{l\sigma} + c_{l-\sigma} c_{i\sigma} \rangle, \end{aligned} \quad (4.5)$$

$$\begin{aligned} E_{24} &= \sum_{\langle l \rangle_i} t e^{i\vec{k} \cdot (\vec{R}_i - \vec{R}_l)} \langle n_{i-\sigma} c_{l\sigma} c_{l-\sigma} + n_{l\sigma} c_{i\sigma} c_{i-\sigma} \rangle \\ &+ \sum_{\langle l \rangle_i} t \langle n_{i\sigma} c_{i-\sigma} c_{l\sigma} - n_{i-\sigma} c_{i\sigma} c_{l-\sigma} \rangle, \end{aligned} \quad (4.6)$$

$$\begin{aligned}
E_{42} = & \sum_{\langle l \rangle_i} t e^{i\vec{k} \cdot (\vec{R}_i - \vec{R}_l)} \left\langle n_{i\sigma} c_{l-\sigma}^\dagger c_{l\sigma}^\dagger + n_{l-\sigma} c_{i-\sigma}^\dagger c_{i\sigma}^\dagger \right\rangle \\
& + \sum_{\langle l \rangle_i} t \left\langle n_{i-\sigma} c_{i\sigma}^\dagger c_{l-\sigma}^\dagger - n_{i\sigma} c_{i-\sigma}^\dagger c_{l\sigma}^\dagger \right\rangle.
\end{aligned} \tag{4.7}$$

These expressions simplify considerably when we introduce the symmetry associated with either singlet or triplet pairing. The anomalous correlation functions are matrix elements between states which differ by the addition of one pair and the spin function associated with a pair is symmetric or antisymmetric for triplet or singlet pairing respectively. It follows that if all spin labels in the correlation function are reversed, i.e. $\sigma \rightarrow -\sigma$, the sign changes in the singlet case but not in the triplet case.

We first consider triplet pairing. Owing to the spin symmetry the second terms in E_{24} and E_{42} vanish and $E_{13} = E_{14} = E_{23} = 0$. Similarly all the elements of the off-diagonal blocks in \mathbf{N}_4 vanish. Furthermore, denoting the correlation function in the first term of E_{24} by β_{il} , we have

$$\begin{aligned}
\beta_{il} &= \langle n_{i-\sigma} c_{l\sigma} c_{l-\sigma} + n_{l\sigma} c_{i\sigma} c_{i-\sigma} \rangle \\
&= \langle n_{i\sigma} c_{l-\sigma} c_{l\sigma} + n_{l-\sigma} c_{i-\sigma} c_{i\sigma} \rangle \\
&= -\langle n_{l-\sigma} c_{i\sigma} c_{i-\sigma} + n_{i\sigma} c_{l\sigma} c_{l-\sigma} \rangle \\
&= -\beta_{li}.
\end{aligned} \tag{4.8}$$

Using this symmetry we write:

$$\beta_{il} = \begin{cases} \beta & \text{for } \vec{R}_i - \vec{R}_l = (a, 0) \\ -\beta & \text{for } \vec{R}_i - \vec{R}_l = (-a, 0) \\ \pm\beta & \text{for } \vec{R}_i - \vec{R}_l = (0, a) \\ \mp\beta & \text{for } \vec{R}_i - \vec{R}_l = (0, -a). \end{cases} \tag{4.9}$$

Thus

$$E_{24} = i\beta_{\vec{k}}, \tag{4.10}$$

where

$$\beta_{\vec{k}} = 2t\beta(\sin k_x a \pm \sin k_y a). \tag{4.11}$$

Similarly

$$E_{42} = -i\beta_{\vec{k}}^*. \tag{4.12}$$

It will be seen shortly that $\beta_{\vec{k}}$ is essentially the gap function and the nodes at $k_x = \pm k_y$ indicate p -wave symmetry. This is as expected for triplet pairing. It is very interesting that the gap is determined not by a simple pair wave function $\langle c_{i-\sigma} c_{l\sigma} \rangle$, but by the more subtle correlation function β_{il} . This quantity cannot be evaluated directly from our Green's functions. The simplest way to evaluate it, and hence obtain a gap equation, is by a factorization procedure described in Sec. V for the case of singlet d -wave pairing. We shall not pursue the p -wave case further here, because this procedure, and others we have investigated, does

not yield a non-zero solution for the gap. The reason for this will be pointed out in Sec. V. We therefore find that p -wave superconductivity does not occur in the 2D Hubbard model.

We now turn to singlet pairing and discuss particularly the case of d -wave symmetry. We defer a discussion of s -wave symmetry to another occasion, partly because we believe it is less likely and partly because the possibility of on-site pairing $\langle c_{i-\sigma} c_{i\sigma} \rangle$ means that all elements E_{nm} in the off-diagonal blocks are non-zero. The d -wave case is simpler because the d -symmetry of the pair wave function ensures that $\langle c_{i-\sigma} c_{i\sigma} \rangle = 0$ and that the summations of the pair wave function $\langle c_{i-\sigma} c_{l\sigma} \rangle$ and of $\langle n_{i\sigma} c_{i-\sigma} c_{l\sigma} \rangle$ over sites l , which are nearest neighbours of site i , give zero. The consistency of these assertions can be checked by expressing these correlation functions in terms of the resultant Green's function. Thus $E_{13} = E_{14} = E_{23} = 0$ and, as in the p -wave case, all elements of the off-diagonal blocks in \mathbf{N}_4 vanish. In a similar way the second terms in E_{24} and E_{42} vanish and we are left with just the first terms of E_{24} and E_{42} , as in the p -wave case. Denoting the correlation function in the first term of E_{24} by γ_{il} , we find, introducing the sign changes on spin reversal in the singlet case, that the equation analogous to Eq. (4.8) is:

$$\gamma_{il} = \langle n_{i-\sigma} c_{l\sigma} c_{l-\sigma} + n_{l\sigma} c_{i\sigma} c_{i-\sigma} \rangle = \gamma_{li}. \quad (4.13)$$

Using the d -wave symmetry we write

$$\gamma_{il} = \begin{cases} \gamma & \text{for } \vec{R}_i - \vec{R}_l = (\pm a, 0) \\ -\gamma & \text{for } \vec{R}_i - \vec{R}_l = (0, \pm a) \end{cases}. \quad (4.14)$$

Hence

$$E_{24} = \gamma_{\vec{k}}, \quad E_{42} = \gamma_{\vec{k}}^*, \quad (4.15)$$

where

$$\gamma_{\vec{k}} = t \sum_{\langle l \rangle_i} e^{i\vec{k} \cdot (\vec{R}_l - \vec{R}_i)} \gamma_{il} = g(\cos k_x a - \cos k_y a) \quad (4.16)$$

with

$$g = 2t\gamma. \quad (4.17)$$

We call $\gamma_{\vec{k}}$ the gap-function and g the gap-function amplitude. The matrices \mathbf{E}_4 and \mathbf{N}_4 now take the partitioned form

$$\mathbf{E}_4 = \begin{bmatrix} \mathbf{E}_2 & 0 & 0 \\ 0 & 0 & \gamma_{\vec{k}} \\ 0 & \gamma_{\vec{k}}^* & -\mathbf{E}_2 \end{bmatrix}, \quad (4.18)$$

$$\mathbf{N}_4 = \begin{bmatrix} \mathbf{N}_2 & \emptyset \\ \emptyset & \mathbf{N}_2 \end{bmatrix}, \quad (4.19)$$

where \mathbf{E}_2 and \mathbf{N}_2 are given by Eqs. (3.1) and (3.2). We shall have a superconducting state if $\gamma_{\vec{k}} \neq 0$ and the central problem we shall presently address is to find a gap equation

satisfied by $\gamma_{\vec{k}}$ and search for a non-zero solution. For the moment we assume $\gamma_{\vec{k}} \neq 0$ and describe how to calculate the Green's function matrix and discuss the general nature of the quasiparticle bands.

The Green's function matrix must be calculated from Eq. (2.14). Here we concentrate on the element $G_{13} = \langle\langle c_{\vec{k}\sigma}; c_{-\vec{k}-\sigma} \rangle\rangle$ from which we can determine the pair wavefunction $\langle c_{i-\sigma} c_{l\sigma} \rangle$. The poles of the Green's function give the quasiparticle bands. It is convenient to partition the matrix $(\omega \mathbf{N}_4 - \mathbf{E}_4)$ into four 2x2 matrices:

$$\omega \mathbf{N}_4 - \mathbf{E}_4 = \begin{bmatrix} A & B \\ C & D \end{bmatrix}. \quad (4.20)$$

Then

$$\mathbf{G}(\omega) = \mathbf{N}_4 (\omega \mathbf{N}_4 - \mathbf{E}_4)^{-1} \mathbf{N}_4 = \begin{bmatrix} \mathbf{N}_2 & \emptyset \\ \emptyset & \mathbf{N}_2 \end{bmatrix} \begin{bmatrix} (A - BD^{-1}C)^{-1} & -A^{-1}B(D - CA^{-1}B)^{-1} \\ -D^{-1}C(A - BD^{-1}C)^{-1} & (D - CA^{-1}B)^{-1} \end{bmatrix} \begin{bmatrix} \mathbf{N}_2 & \emptyset \\ \emptyset & \mathbf{N}_2 \end{bmatrix} \quad (4.21)$$

and the calculation of G_{13} only involves the upper right-hand block $-A^{-1}B(D - CA^{-1}B)^{-1}$. It is now straightforward to show that

$$G_{13}(\omega) = -\gamma_{\vec{k}}(E_{12} - nE_{11})^2/D(\omega), \quad (4.22)$$

where

$$\begin{aligned} D(\omega) &= \det(\mathbf{N}_4\omega - \mathbf{E}_4) \\ &= ((\omega - E_{11})(\omega n - E_{22}) - (\omega n - E_{12})^2) \\ &\quad \times ((\omega + E_{11})(\omega n + E_{22}) - (\omega n + E_{12})^2) \\ &\quad - \gamma_{\vec{k}}^* \gamma_{\vec{k}}(\omega^2 - E_{11}^2). \end{aligned} \quad (4.23)$$

E_{11} , E_{12} and E_{22} may be substituted from Eq. (3.1) and we find

$$G_{13}(\omega) = -\gamma_{\vec{k}}(n(1-n)U)^2/D(\omega). \quad (4.24)$$

The quasiparticle bands in the superconducting state satisfy $D(\omega) = 0$ and we denote them by $\omega = \pm E_{1\vec{k}}$, $\omega = \pm E_{2\vec{k}}$, with $E_{2\vec{k}} > E_{1\vec{k}} > 0$. Thus

$$D(\omega) = n^2(1-n)^2(\omega^2 - E_{1\vec{k}}^2)(\omega^2 - E_{2\vec{k}}^2). \quad (4.25)$$

When $|\gamma_{\vec{k}}|/n(1-n) \ll \sqrt{\xi_{2\vec{k}}^2 - \xi_{1\vec{k}}^2}$, we have

$$E_{1\vec{k}}^2 = \xi_{1\vec{k}}^2 + \frac{|\gamma_{\vec{k}}|^2}{n^2(1-n)^2} \frac{E_{11}^2 - \xi_{1\vec{k}}^2}{\xi_{2\vec{k}}^2 - \xi_{1\vec{k}}^2}, \quad (4.26)$$

$$E_{2\vec{k}}^2 = \xi_{2\vec{k}}^2 + \frac{|\gamma_{\vec{k}}|^2}{n^2(1-n)^2} \frac{\xi_{2\vec{k}}^2 - E_{11}^2}{\xi_{2\vec{k}}^2 - \xi_{1\vec{k}}^2}, \quad (4.27)$$

and, from Eq. (3.1), $E_{1\vec{k}} = \epsilon_{\vec{k}} + Un - \mu$. Here $\xi_{1\vec{k}}, \xi_{2\vec{k}}$ with $\xi_{1\vec{k}} < \xi_{2\vec{k}}$ are the quasiparticle bands in the normal state given by Eq. (3.10). The form of $E_{1\vec{k}}^2$ is familiar from BCS-theory and the superconducting gap at points \vec{k} on the normal state Fermi surface $\xi_{1\vec{k}} = 0$ is given by $|\Delta_{\vec{k}}|$ where, combining Eq. (4.16) and Eq. (4.26),

$$\Delta_{\vec{k}} = \frac{g(\cos k_x a - \cos k_y a)}{n(1-n)} \cdot \frac{(\epsilon_{\vec{k}} + Un - \mu)}{\xi_{2\vec{k}}}. \quad (4.28)$$

The \vec{k} -dependence of $\Delta_{\vec{k}}$ is entirely due to the $(\cos k_x a - \cos k_y a)$ -factor, since the second factor is constant over the Fermi surface. So, over the Fermi surface,

$$\Delta_{\vec{k}} = G(\cos k_x a - \cos k_y a), \quad (4.29)$$

with

$$G = \frac{g(\epsilon_{\vec{k}_F} + Un - \mu)}{n(1-n)\xi_{2\vec{k}_F}}. \quad (4.30)$$

We call G the gap amplitude. Recall that we call g , introduced in Eq. (4.17), the gap-function amplitude. G tends to $g/(1-n)$ as $U \rightarrow \infty$. Examples of quasiparticle bands in the superconducting state are given later in Fig. 6, with the gap-function amplitude g determined by a method described in Sec. V.

In calculations which relate to the superconducting state it is reasonable to assume that $W_{\vec{k}}$, which appears in the matrix \mathbf{E}_2 [whose elements appear in Eq. (4.24)], takes the values it has in the normal state (where $\gamma_{\vec{k}} = 0$) at $T = 0$. Thus the effect of superconductivity on the quasiparticle bands, and the temperature dependence of these bands, is entirely due to the gap function $\gamma_{\vec{k}}$. The correlation function $\langle c_{-\vec{k}-\sigma} c_{\vec{k}\sigma} \rangle$ is related to $G_{13}(\omega)$ by the use of Eq. (2.15) so that, using Eq. (4.24) and Eq. (4.25),

$$\langle c_{-\vec{k}-\sigma} c_{\vec{k}\sigma} \rangle = \frac{1}{2\pi i} \oint f(\omega) \frac{-\gamma_{\vec{k}} U^2}{(\omega^2 - E_{1\vec{k}}^2)(\omega^2 - E_{2\vec{k}}^2)} d\omega. \quad (4.31)$$

Hence

$$\langle c_{-\vec{k}-\sigma} c_{\vec{k}\sigma} \rangle = -\gamma_{\vec{k}} U^2 F(E_{1\vec{k}}, E_{2\vec{k}}), \quad (4.32)$$

where

$$F(a, b) = \frac{1}{2(b^2 - a^2)} \left[\frac{\tanh\left(\frac{1}{2}\beta a\right)}{a} - \frac{\tanh\left(\frac{1}{2}\beta b\right)}{b} \right]. \quad (4.33)$$

At $T = 0$ ($\beta \rightarrow \infty$) this becomes

$$\langle c_{-\vec{k}-\sigma} c_{\vec{k}\sigma} \rangle = \frac{-\gamma_{\vec{k}} U^2}{2E_{1\vec{k}} E_{2\vec{k}} (E_{1\vec{k}} + E_{2\vec{k}})}. \quad (4.34)$$

The pair wave function in real space may then be calculated using the relation

$$\langle c_{i-\sigma} c_{l\sigma} \rangle = \frac{1}{L} \sum_{\vec{k}} e^{i\vec{k} \cdot (\vec{R}_i - \vec{R}_l)} \langle c_{-\vec{k}-\sigma} c_{\vec{k}\sigma} \rangle. \quad (4.35)$$

V. THE GAP EQUATION

In the d -wave case the gap is determined by the gap-function $\gamma_{\vec{k}}$ and we need a self-consistent way of finding the gap-function amplitude g which appears in Eq. (4.16). As pointed out in the previous section the gap is not determined by a simple pair wave function $\langle c_{i-\sigma} c_{l\sigma} \rangle$, but by the correlation function γ_{il} given by Eq. (4.13), which may be written as

$$\gamma_{il} = \left\langle \left(c_{i-\sigma}^\dagger c_{l-\sigma} + c_{l\sigma}^\dagger c_{i\sigma} \right) c_{i-\sigma} c_{l\sigma} \right\rangle. \quad (5.1)$$

In the d -wave case this may also be written as

$$\gamma_{il} = \left\langle c_{i\sigma}^\dagger c_{l\sigma} c_{l-\sigma} c_{i\sigma} \right\rangle + \left\langle c_{l\sigma}^\dagger c_{i\sigma} c_{i-\sigma} c_{l\sigma} \right\rangle, \quad (5.2)$$

which shows explicitly that $\gamma_{il} = \gamma_{li}$. This is not expressible directly in terms of our Green's functions and various possibilities suggest themselves. A satisfactory procedure might be to extend the formalism to two-particle Green's functions as suggested in connection with the correlation functions appearing in w_1 , Eq. (3.6). This remains to be investigated. Alternatively we can follow the procedure we adopted, following Roth, for the latter correlation functions and introduce additional Green's functions containing one- and three-particle operators. This is the method we shall use here, since it is consistent with our treatment of the normal state which, by comparison with Monte Carlo results, has been shown to work well. However there is one complication. Whereas for the correlation functions appearing in the normal paramagnetic state the procedure is unambiguous,²³ this is not so for γ_{il} . The four-operator correlation function may be related to a Green's function containing a one- and three-particle operator in four ways and in the case of γ_{il} these are distinct and yield different results. It is sufficient to consider one of the correlation functions in Eq. (5.2). Thus $\langle c_{l\sigma}^\dagger c_{i\sigma} c_{i-\sigma} c_{l\sigma} \rangle$ may be calculated using any of the following Green's functions:

$$\begin{aligned} \text{(a)} \quad & \left\langle \left\langle c_{i\sigma}; c_{l\sigma}^\dagger c_{i-\sigma} c_{l\sigma} \right\rangle \right\rangle, & \text{(b)} \quad & \left\langle \left\langle c_{i-\sigma}; c_{l\sigma}^\dagger c_{i\sigma} c_{l\sigma} \right\rangle \right\rangle, \\ \text{(c)} \quad & \left\langle \left\langle c_{l\sigma}; c_{l\sigma}^\dagger c_{i\sigma} c_{i-\sigma} \right\rangle \right\rangle, & \text{(d)} \quad & \left\langle \left\langle c_{l\sigma}^\dagger; c_{i\sigma} c_{i-\sigma} c_{l\sigma} \right\rangle \right\rangle. \end{aligned}$$

Use of (a) or (b) splits up the product $c_{i\sigma} c_{i-\sigma}$ and therefore does not preserve the important result that $\gamma_{il} \rightarrow 0$ when site double occupation is suppressed as $U \rightarrow \infty$. Consequently both of these procedures, which yield similar but not identical results, fail at large U and are generally expected to overestimate the gap. This result is closely related to the factorization $\langle c_{l\sigma}^\dagger c_{i\sigma} c_{i-\sigma} c_{l\sigma} \rangle = \langle c_{l\sigma}^\dagger c_{i\sigma} \rangle \langle c_{i-\sigma} c_{l\sigma} \rangle$ and in fact use of (a) or (b) is exactly equivalent to this factorization as $U \rightarrow \infty$. Rather than use (a) or (b) precisely we develop the related factorization method in Sec. V A. This has the advantage of simplicity and shows clearly the structure of the gap equation and why d -wave pairing occurs and p -wave pairing does not. Although it fails for large U , we believe it is useful in providing an upper estimate of the gap and T_c at finite, intermediate U .

Use of the Green's functions (c) or (d) preserves the property $\gamma_{il} \rightarrow 0$ as $U \rightarrow \infty$ and is therefore the preferred procedure for large U . At smaller U it seems likely that the correct results may lie between those obtained from (c) or (d) and those from (a), (b), or the factorization procedure. We therefore regard the gap and T_c obtained using (c) or (d) as a lower estimate of those quantities. It is remarkable that although analyses using (c) and (d) are formally different the numerical results for the gap are almost identical. In Sec. V B we

will therefore give details of the gap equation for case (c) only. Of the four possibilities (c) has the advantage of giving the correct $U \rightarrow \infty$ limit for the correlation function and of a more balanced distribution of creation and destruction operators than (d).

There is a reassuring consistency in that all the procedures discussed yield d -wave pairing, not p -wave pairing, and in all cases the gap and T_c as function of site occupation $\langle N \rangle$ are sharply peaked at an optimum doping corresponding to the square Fermi surface $\epsilon_{\vec{k}} = 0$. These results are presented in Secs. V A and V B for the two basic methods which provide upper and lower estimates of the magnitude of the gap and T_c .

A. The factorization procedure

The factorization procedure approximates γ_{il} , given by Eq. (5.1), as

$$\gamma_{il} = \left(\langle c_{i-\sigma}^\dagger c_{l-\sigma} \rangle + \langle c_{l\sigma}^\dagger c_{i\sigma} \rangle \right) \langle c_{i-\sigma} c_{l\sigma} \rangle. \quad (5.3)$$

The symmetry $\gamma_{il} = \gamma_{li}$ is retained but, as discussed above, the products $c_{i\sigma} c_{l-\sigma}$ and $c_{l-\sigma} c_{i\sigma}$ are split up so that in general γ_{il} does not tend to zero when site double occupation is suppressed as $U \rightarrow \infty$. However the averages $\langle c_{l-\sigma} c_{i\sigma} \rangle$ are always zero due to d -wave symmetry, so that double occupation within a pair is suppressed, but not between pairs. In the special case of half-filling ($\langle N \rangle = 1$), $\gamma_{il} \rightarrow 0$ as $U \rightarrow \infty$, because the correlations $\langle c_{i-\sigma}^\dagger c_{l-\sigma} \rangle$ and $\langle c_{l\sigma}^\dagger c_{i\sigma} \rangle$ tend to zero. We may rewrite Eq. (5.3) as

$$\gamma_{il} = 2n_1 \langle c_{i-\sigma} c_{l\sigma} \rangle, \quad (5.4)$$

where

$$n_1 = \langle c_{i-\sigma}^\dagger c_{l-\sigma} \rangle = \langle c_{l\sigma}^\dagger c_{i\sigma} \rangle. \quad (5.5)$$

It is straightforward to show that

$$n_1 t = \frac{1}{zL} \sum_{\vec{k}} \epsilon_{\vec{k}} n_{\vec{k}}, \quad (5.6)$$

where $n_{\vec{k}} = \langle c_{\vec{k}\sigma}^\dagger c_{\vec{k}\sigma} \rangle$ and z is the number of nearest neighbours, i.e. $z = 4$ for the 2D square lattice.

We are now in a position to find the equation which determines the gap-function amplitude g in Eq. (4.16) self-consistently. From Eqs. (4.16) and (5.4) we get

$$\gamma_{\vec{k}} = 2n_1 t \sum_{\langle l \rangle_i} \cos [\vec{k} \cdot (\vec{R}_i - \vec{R}_l)] \langle c_{i-\sigma} c_{l\sigma} \rangle. \quad (5.7)$$

By using Eqs. (4.32) and (4.35) we find:

$$\gamma_{\vec{k}} = -\frac{2n_1 t U^2}{L} \sum_{\langle l \rangle_i} \cos [\vec{k} \cdot (\vec{R}_i - \vec{R}_l)] \sum_{\vec{q}} \gamma_{\vec{q}} \cos [\vec{q} \cdot (\vec{R}_i - \vec{R}_l)] F(E_{1\vec{q}}, E_{2\vec{q}}). \quad (5.8)$$

Clearly the quasiparticle energies $E_{1\vec{q}}$, $E_{2\vec{q}}$ are symmetric in q_x and q_y , because they satisfy the equation $D(\omega)=0$, where $D(\omega)$ is defined by Eq. (4.23) and $|\gamma_{\vec{q}}|^2$ and the elements of \mathbf{E}_2 have this symmetry. Now substituting Eq. (4.16),

$$\gamma_{\vec{q}} = g (\cos q_x a - \cos q_y a) , \quad (5.9)$$

into Eq. (5.8) and exploiting the symmetry between q_x and q_y , we find:

$$\gamma_{\vec{k}} = -\gamma_{\vec{k}} \frac{2n_1 t U^2}{L} \sum_{\vec{q}} (\cos q_x a - \cos q_y a)^2 F(E_{1\vec{q}}, E_{2\vec{q}}) . \quad (5.10)$$

Thus for a non-zero solution $\gamma_{\vec{k}}$ must satisfy the gap equation

$$1 = -\frac{2n_1 t U^2}{L} \sum_{\vec{k}} (\cos k_x a - \cos k_y a)^2 F(E_{1\vec{k}}, E_{2\vec{k}}) , \quad (5.11)$$

where $\gamma_{\vec{k}}$ is contained in the quasiparticle energies $E_{1\vec{k}}, E_{2\vec{k}}$. At $T = 0$, $F(a, b)$ takes the form $[2ab(a+b)]^{-1}$, so that the gap equation becomes:

$$1 = -\frac{n_1 t U^2}{L} \sum_{\vec{k}} \frac{(\cos k_x a - \cos k_y a)^2}{E_{1\vec{k}} E_{2\vec{k}} (E_{1\vec{k}} + E_{2\vec{k}})} . \quad (5.12)$$

Since $\sum_{\vec{k}} \epsilon_{\vec{k}} = 0$ and $n_{\vec{k}}$ is a monotonically decreasing function of $\epsilon_{\vec{k}}$, it follows from Eq. (5.6) that $n_1 t < 0$. Also $E_{2\vec{k}} > E_{1\vec{k}} > 0$, so that a solution with $g \neq 0$ may occur. At finite temperature T Eq. (5.11) determines g as a function of temperature, and hence the critical temperature T_c where $g = 0$. Eq. (5.12) has a rather BCS-like form, particularly if we allow ourselves to consider large U where $E_{2\vec{k}} \sim U$ and the factor $E_{2\vec{k}} (E_{1\vec{k}} + E_{2\vec{k}})$ in the denominator in Eq. (5.12) cancels with the factor U^2 in the numerator. In this approximation the superconductivity is driven by the kinetic energy term $-n_1 t$, but for large U , where the approximation of Sec. VB is more appropriate, this is effectively replaced by a quantity of order t^2/U .

In the case of p -wave pairing, which was briefly considered in Sec. IV, the equation corresponding to Eq. (5.12) is of the form

$$1 = \frac{n_1 t U^2}{L} \sum_{\vec{k}} \frac{(\sin k_x a \pm \sin k_y a)^2}{E_{1\vec{k}} E_{2\vec{k}} (E_{1\vec{k}} + E_{2\vec{k}})} . \quad (5.13)$$

The right-hand side is now negative and no solution is possible. The change of sign from the d -wave case is due to the factor i in Eq. (4.10), which does not appear in Eq. (4.15). Thus p -wave superconductivity does not occur.

As mentioned earlier, in calculating superconducting properties such as the gap amplitude and its temperature dependence we neglect the unimportant temperature dependence of n_1 and $W_{\vec{k}}$ and evaluate these with $g = 0$ and $T = 0$. The d -wave gap amplitude G at $T = 0$ over the Fermi surface calculated from Eqs. (5.12) and (4.30) is shown in Fig. 7 as a function of occupation $\langle N \rangle$ for different values of $U/|t|$. Clearly, from Eq. (4.28) the maximum gap occurs at points on the Fermi-surface where $k_x = 0$ or $k_y = 0$. For each $U/|t|$

the gap maximum, corresponding to optimum doping, occurs for the occupation which has the square Fermi surface $\epsilon_{\vec{k}} = 0$. The flat saddle-point feature of the normal state quasiparticle bands (Fig. 1) around $(\pi, 0)$ then lies precisely at the Fermi level. If the occupation is increased (underdoping with holes) the saddle-point lies below the Fermi level and the Fermi surface is a closed hole-like one around (π, π) . For overdoping the saddle-point lies above the Fermi level and the Fermi surface is a closed electron-like one around $(0, 0)$. This situation is unchanged in the approximation of Sec. VB, which is more appropriate for large U . It has close similarities with the van Hove scenario of Newns *et al.*²¹ and has implications for transport properties which we explore in the discussion section.

Quasiparticle bands in the superconducting state are obtained by solving the equation $D(\omega) = 0$, where $D(\omega)$ is given by Eq. (4.23) and the bands are given to a good approximation by Eqs. (4.26) and (4.27). Examples of these bands are shown in Fig. 6. The upper Hubbard bands $\omega = \pm E_{2\vec{k}}$ are too far from the Fermi level to appear in this figure.

In Fig. 8 we print the values of the pair wave function $\langle c_{i-\sigma} c_{l\sigma} \rangle$, calculated from Eq. (4.35), for several $\vec{R}_i - \vec{R}_l$ on the lattice. It turns out that for optimum doping the pair wave function is strongly peaked if i and l are neighbouring sites. Away from optimum doping this peak is less pronounced and the pair wave function extends over several lattice sites. This behaviour of the pair wave function reflects the local nature of the pairing mechanism.

The temperature dependence of the gap-function amplitude $g(T)$ is calculated from Eq. (5.11) and in Fig. 9 results for $G(T)$ are shown for $U/|t| = 12$ and various occupations including the optimum doping case of $\langle N \rangle = 0.76$. It is clear from Fig. 9 that $2\Delta_{max}/k_B T_c \sim 4$ for optimum doping and under-doping, but larger for overdoping. The units of g and $k_B T$ in Figs. 7 and 9 are $2|t|$, so that if $|t|$ takes a reasonable value of 0.5 eV, the units are eV. Then T_c at optimum doping for $U/|t| = 12$ is 125 K. As discussed earlier we regard these results for the gap and T_c as upper bound estimates. They are strongly reduced in the approximation of the next section, which we believe yields lower bound estimates, but the qualitative behaviour is unchanged.

B. A gap equation valid for large U

As discussed above, we obtain a gap equation by writing the correlation functions which appear in Eq. (5.2) as

$$\langle c_{l\sigma}^\dagger c_{i\sigma} c_{i-\sigma} c_{l\sigma} \rangle = \langle \hat{B}_{li} c_{l\sigma} \rangle, \quad (5.14)$$

with

$$\hat{B}_{li} = c_{l\sigma}^\dagger c_{i\sigma} c_{i-\sigma}, \quad (5.15)$$

and thus expressing it in terms of the Green's function $\langle \langle c_{l\sigma}; \hat{B}_{li} \rangle \rangle$. From Eq. (5.2) we have

$$\gamma_{il} = \langle \hat{B}_{il} c_{i\sigma} \rangle + \langle \hat{B}_{li} c_{l\sigma} \rangle. \quad (5.16)$$

It is convenient to introduce Bloch operators by writing

$$\langle \hat{B}_{li} c_{l\sigma} \rangle = L^{-1/2} \sum_{\vec{k}} e^{-i\vec{k} \cdot \vec{R}_l} \langle \hat{B}_{li} c_{\vec{k}\sigma} \rangle. \quad (5.17)$$

Also, using Eqs. (2.11) and (2.15) and noting that $\hat{A}_{1\vec{k}\sigma} = c_{\vec{k}\sigma}$ we have

$$\langle \hat{B}_{li} c_{\vec{k}\sigma} \rangle = \sum_m I_m(\vec{k}) \left\langle [\hat{A}_{m\vec{k}\sigma}, \hat{B}_{li}]_+ \right\rangle, \quad (5.18)$$

where

$$I_m(\vec{k}) = \frac{1}{2\pi i} \oint f(\omega) \tilde{G}_{1m}(\vec{k}, \omega) d\omega. \quad (5.19)$$

It is straightforward to show that

$$\left\langle [\hat{A}_{1\vec{k}\sigma}, \hat{B}_{li}]_+ \right\rangle = 0, \quad (5.20)$$

$$\left\langle [\hat{A}_{2\vec{k}\sigma}, \hat{B}_{li}]_+ \right\rangle = L^{-1/2} e^{i\vec{k} \cdot \vec{R}_l} \langle n_{l-\sigma} c_{i\sigma} c_{i-\sigma} \rangle, \quad (5.21)$$

$$\left\langle [\hat{A}_{3\vec{k}\sigma}, \hat{B}_{li}]_+ \right\rangle = L^{-1/2} e^{i\vec{k} \cdot \vec{R}_i} n_1, \quad (5.22)$$

$$\begin{aligned} \left\langle [\hat{A}_{4\vec{k}\sigma}, \hat{B}_{li}]_+ \right\rangle &= L^{-1/2} e^{i\vec{k} \cdot \vec{R}_i} (n_1 - m_1) \\ &\quad + L^{-1/2} e^{i\vec{k} \cdot \vec{R}_l} \langle c_{l-\sigma}^\dagger c_{l\sigma}^\dagger c_{i\sigma} c_{i-\sigma} \rangle, \end{aligned} \quad (5.23)$$

where n_1 is defined by Eq. (5.5) and, similarly,

$$m_1 = \langle c_{l\sigma}^\dagger n_{i-\sigma} c_{i\sigma} \rangle = \langle c_{i\sigma}^\dagger n_{l-\sigma} c_{l\sigma} \rangle. \quad (5.24)$$

So m_1 can be calculated straightforwardly from G_{12} and it is sufficient to use its value in the normal state at $T = 0$. This may be written as

$$m_1 t = \frac{n}{zL} \sum_{\vec{k}} \epsilon_{\vec{k}} \frac{W_{\vec{k}} - \xi_{1\vec{k}}}{\xi_{2\vec{k}} - \xi_{1\vec{k}}} f(\xi_{1\vec{k}}) \quad (5.25)$$

in the case when only the lower quasiparticle band is occupied. It is important to note that for large U , $m_1 t \sim t^2/U$, whereas $n_1 t \sim t$. The expressions for \tilde{G}_{1m} are obtained in a similar way to that used to find G_{13} in Sec. IV. We find

$$\tilde{G}_{12} = Un^2(1-n)^2 (\omega + \xi_{1\vec{k}}) (\omega + \xi_{2\vec{k}}) / D(\omega), \quad (5.26)$$

$$\tilde{G}_{13} = -\gamma_{\vec{k}} Un^2(1-n) (\omega + \epsilon_{\vec{k}} - \mu + U) / D(\omega), \quad (5.27)$$

$$\tilde{G}_{14} = \gamma_{\vec{k}} Un(1-n) (\omega + \epsilon_{\vec{k}} - \mu + Un) / D(\omega). \quad (5.28)$$

We note also that for d -wave symmetry the correlation function on the right of Eq. (5.21) is equal to $\langle \hat{B}_{li} c_{l\sigma} \rangle$. It is also important to note that, owing to the factors $\gamma_{\vec{k}}$ in Eqs. (5.27) and (5.28), $I_3(\vec{k})$ and $I_4(\vec{k})$ change sign under interchange of k_x and k_y . Consequently on substituting for the correlation functions on the right of Eq. (5.18) from Eqs. (5.20)-(5.23) and substituting the result in Eq. (5.17), we find that the contribution from the second term on the right of Eq. (5.23) vanishes on summing over \vec{k} . The result is

$$\langle \hat{B}_{li} c_{l\sigma} \rangle = \frac{C}{L} \sum_{\vec{k}} e^{i\vec{k} \cdot (\vec{R}_i - \vec{R}_l)} \left[I_3(\vec{k}) n_1 + I_4(\vec{k}) (n_1 - m_1) \right], \quad (5.29)$$

where

$$C = \left[1 - L^{-1} \sum_{\vec{q}} I_2(\vec{q}) \right]^{-1}. \quad (5.30)$$

It follows from Eqs. (4.16) and (5.16) that

$$\gamma_{\vec{k}} = \frac{2tC}{L} \sum_{\langle l \rangle_i} \cos [\vec{k} \cdot (\vec{R}_i - \vec{R}_l)] \sum_{\vec{q}} \gamma_{\vec{q}} \cos [\vec{q} \cdot (\vec{R}_i - \vec{R}_l)] \frac{I_3(\vec{q}) n_1 + I_4(\vec{q}) (n_1 - m_1)}{\gamma_{\vec{q}}}. \quad (5.31)$$

This is of the same form as Eq. (5.8) and, on using Eq. (5.9) as before, we find the gap equation

$$\frac{L}{2tC} = \sum_{\vec{k}} (\cos k_x a - \cos k_y a)^2 \frac{I_3(\vec{k}) n_1 + I_4(\vec{k}) (n_1 - m_1)}{\gamma_{\vec{k}}} \quad (5.32)$$

It is sufficient to evaluate the constant C in the normal state at $T = 0$ and we find

$$C = \left[1 + UL^{-1} \sum_{\vec{k}} (\xi_{2\vec{k}} - \xi_{1\vec{k}})^{-1} \theta(-\xi_{1\vec{k}}) \right]^{-1}, \quad (5.33)$$

where $\theta(x) = 1$ if $x > 0$ and $= 0$ otherwise. As $U \rightarrow \infty$, $C \rightarrow 1 - n$. At $T = 0$, using Eqs. (5.26)-(5.28) and Eq. (5.19), we obtain the gap equation in the form

$$1 = -\frac{UtC}{n(1-n)L} \sum_{\vec{k}} (\cos k_x a - \cos k_y a)^2 \frac{[(1-n)n_1 - m_1] (\mu - \epsilon_{\vec{k}}) + Um_1 n}{E_{1\vec{k}} E_{2\vec{k}} (E_{1\vec{k}} + E_{2\vec{k}})}. \quad (5.34)$$

This is similar in form to the gap equation, Eq. (5.12), obtained using the factorization method. Both terms in the numerator of the last factor of Eq. (5.34) are of order t , since $m_1 \sim t/U$. If we were to retain only the $Um_1 n$ term and take $C = 1 - n$, its value at $U = \infty$, we would obtain the form of Eq. (5.12) exactly, but with m_1 replacing n_1 . Thus, from the discussion following Eq. (5.12), superconductivity at large U is driven by a term of order t^2/U . This seen clearly in Fig. 10, where the gap amplitude G over the Fermi surface is plotted as a function of occupation $\langle N \rangle$ for different values of $U/|t|$. The peak value of G , corresponding to optimum doping with the square Fermi surface as before, increases rapidly with decreasing $U/|t|$. At $U = 4|t|$ the peak value is about one tenth of the rather constant peak value (see Fig. 7) found by the factorization procedure. Qualitatively nothing is changed and the quasiparticle bands are just like those of Fig. 6, but with a smaller gap. The temperature dependence of the gap amplitude $g(T)$ is calculated from Eq. (5.32) and in Fig. 11 the result for $G(T)$ is shown for $U = 4|t|$ at optimum doping. If $|t| = 0.5\text{eV}$ the corresponding T_c is 10K.

As discussed earlier we expect the correct values for the gap and T_c to lie somewhere between the values obtained from the two approximations used. Thus for the physically reasonable parameters $|t| = 0.5\text{eV}$, $U = 2\text{eV}$, we have shown that d -wave superconductivity occurs with T_c in the range 10 – 100K at optimum doping $\delta_c = 0.14$.

VI. CONCLUSIONS

We have systematically applied Roth's decoupling method²³ to the two dimensional Hubbard model, investigating both the normal and superconducting states. Although there are intrinsic defects in the method we believe we are able to draw some significant conclusions. In the normal state the method corresponds to a two-pole approximation to the one-particle Green's function, so that for a given wave-vector \vec{k} and spin σ the spectral function consists of two delta-function peaks, the sum of whose weights is unity, corresponding to states in the upper and lower Hubbard bands. For site occupation $\langle N \rangle < 1$ only the lower band is occupied and the absence of any incoherent spectral weight below the Fermi level necessarily implies a Fermi surface of volume greater than that appropriate to a non-interacting system or Fermi liquid. Nevertheless we have shown in Sec. III that there is very remarkable agreement between calculated bands and those obtained in Monte Carlo calculations by Bulut *et al.*;²⁴ in particular for $U = 8|t|$ and several values of $\langle N \rangle$ the position of the Fermi level, and hence the nature the Fermi surface, is in agreement. This implies that for $\langle N \rangle \gtrsim 0.8$ the anomalous Fermi surface volume is not merely a result of the Roth approximation, but is a real effect. This could be caused by the finite temperature in the Monte Carlo calculations, but can possibly also be explained on the basis of the Edwards-Hertz theory,^{42,43} in which for U larger than the bandwidth, a transition from a Fermi liquid to a non-Fermi liquid with enlarged Fermi surface volume occurs as $\langle N \rangle$ increases through a critical value N_c . However the two-pole approximation omits the quasiparticle lifetime broadening which, in the Edwards-Hertz theory occurs even at the Fermi level for $\langle N \rangle > N_c$. Our calculated bands also feature almost dispersionless bands around the $(\pi, 0)$ points as is observed in recent ARPES experiments on hole doped cuprate superconductors.³⁶⁻⁴⁰ Another feature our calculations share with experiments^{44,45} is the weight transfer from the upper to the lower band upon doping. For intermediate U this transfer is \vec{k} -dependent and has a maximum at the (π, π) point.

In Sec. V it is shown how d -wave superconductivity, but not p -wave, occurs. An important conclusion is that reasonable transition temperatures, in the range 10 – 100K, only occur for $U \lesssim 6|t|$ and in a fairly small range of occupation $\langle N \rangle$ near optimum doping where the saddle-point feature of the quasiparticle band structure at $(\pi, 0)$ is placed at the Fermi level. For $U \lesssim 6|t|$ the system is expected to be a Fermi liquid for all $\langle N \rangle$, so that the anomalous volume of the Fermi surface is spurious in this regime. However this defect of the method is rather fortunate since it enables us to obtain the saddle-point feature of the band at the Fermi level for a doped case ($\langle N \rangle < 1$) without recourse to next nearest neighbour hopping. Also the absence of lifetime broadening in the two-pole approximation is a correct feature near the Fermi level in the Fermi liquid regime. We therefore believe our results are significant and closely parallel the Monte Carlo results of Husslein *et al.*²⁰ on d -wave superconductivity in the tt' Hubbard model. The association of optimum doping with a saddle-point at the Fermi level (see also Ref. 21) is consistent with the generically different behaviour of doped superconducting cuprates in many normal state properties at exactly optimum doping, as opposed to those at under- or overdoping. It is well known²¹ that a saddle-point at the Fermi level leads to marginal Fermi liquid transport properties such as a normal state resistivity varying linearly with temperature. A recent discussion of thermopower⁵⁰ strengthens the case for the van Hove scenario in the cuprate superconductors.

Even though the method of Sec. VB still gives superconductivity near optimum doping for $U > 8|t|$, but with very low T_c , it is unlikely that the superconducting state would survive the introduction of finite quasiparticle lifetimes at the Fermi level which might arise from non-Fermi liquid behaviour in this region.

The present work suggests that high temperature superconductivity arises in moderately correlated systems which may be doped so that the Fermi level approaches a van Hove singularity in the quasiparticle band structure. Correlation helps by flattening the bands, accentuating the singularity, but must not be allowed to reduce site double occupation too markedly. Nearest neighbour antiferromagnetic correlations are particularly important both in flattening the bands and in promoting double occupation. The correlations important for superconductivity in the present model are local ones and the mechanism is different from spin-fluctuation-exchange models.

In future work we propose to explore the possibility of s -wave pairing, particularly its degree of anisotropy if it is found to occur. Work is in progress on extending the Roth method consistently to two-particle Green's functions, particularly with the aim of calculating the dynamical susceptibility $\chi(\vec{q}, \omega)$ and investigating the spin dynamics of the system.

ACKNOWLEDGMENTS

One of us (J.B.) thankfully acknowledges financial support from the SERC, the 'Universiteitsfonds Twente', the British Council and the Commission of the European Community during the course of this work.

REFERENCES

- ¹ J. Bardeen, L.N. Cooper, and J.R. Schrieffer, Phys. Rev. **106**, 162 (1957).
- ² J.G. Bednorz and K.A. Müller, Z. Phys. B **64**, 189 (1986).
- ³ C.E. Gough *et al.*, Nature **326**, 855 (1987).
- ⁴ C.C. Tsuei *et al.*, Phys. Rev. Lett. **73**, 593 (1994).
- ⁵ L.N. Vu *et al.*, Appl. Phys. Lett. **63**, 1693 (1993).
- ⁶ J.E. Sonier *et al.*, Phys. Rev. Lett. **72**, 744 (1993).
- ⁷ Z.X. Shen *et al.*, Phys. Rev. Lett. **70**, 1553 (1993).
- ⁸ A.J. Leggett, Physica B **199 & 200** 291 (1994).
- ⁹ P.W. Anderson, Science **235**, 1196 (1987).
- ¹⁰ J. Hubbard, Proc. Royal Soc. London **A 276**, 238 (1963).
- ¹¹ F.C. Zhang and T.M. Rice, Phys. Rev. B **37**, 3759 (1988).
- ¹² H. Eskes and G.A. Sawatzky, Phys. Rev. Lett. **61**, 1415 (1988).
- ¹³ P.W. Anderson, Physica B **199 & 200**, 8 (1994).
- ¹⁴ Z.Z. Sheng and A.M. Hermann, Nature **332**, 138 (1988); R.N. Shelton, in *High Temperature Superconductivity*, edited by J.W. Lynn (Springer-Verlag, New York, 1990).
- ¹⁵ P. Monthoux and D.Pines, Phys. Rev. B **49**, 4261 (1994); D. Pines, Physica B **199 & 200**, 300 (1994).
- ¹⁶ N.E. Bickers, D.J. Scalapino, and S.R. White, Phys. Rev. Lett. **62**, 961 (1989).
- ¹⁷ K.Ueda, T. Moriya, and Y. Takahashi, J. Phys. Chem. Solids **53**, 1515 (1992).
- ¹⁸ P.W. Anderson, Physics Today **47** no.2, 11 (1994).
- ¹⁹ W. von der Linden, Physics Reports **220**, 53 (1992).
- ²⁰ T. Husslein, I. Morgenstern, D.M. Newns, P.C. Pattnaik, J.M. Singer, and H.G. Matuttis, (to be published).
- ²¹ D.M. Newns, C.C. Tsuei, P.C. Pattnaik, and C.L. Kane, Comments Cond. Mat. Phys. **15**, 273 (1992); D.M. Newns, H.R. Krishnamurthy, P.C. Pattnaik, C.C. Tsuei, C.C. Chi and C.L. Kane, Physica B **186-188**, 801-807 (1993).
- ²² J. Linderberg and Y. Öhrn, Chem. Phys. Lett. **1**, 295 (1967).
- ²³ L.M. Roth, Phys. Rev. **184**, 451 (1969).
- ²⁴ N. Bulut, D.J. Scalapino, and S.R. White, Phys. Rev. B **50**, 7215 (1994); Phys. Rev. Lett. **73**, 748 (1994).
- ²⁵ E. Dagotto, A. Nazarenko, and A. Moreo, Phys. Rev. Lett. **74**, 310 (1994).
- ²⁶ J. Beenen and D.M. Edwards (unpublished).
- ²⁷ K. Eapen, J. Phys. C: Solid State Phys. **15**, 6007 (1982).
- ²⁸ U. Lindner and A.C. Hewson, Phys. Status Solidi B **62**, 603 (1974).
- ²⁹ H. Mori, Prog. Theor. Phys. **33**, 423 (1965); R. Zwanzig, Phys. Rev. **124**, 983 (1961).
- ³⁰ P. Fulde, in *Electron Correlations in Molecules and Solids* (Springer Series in Solid State, Vol. 100, 1991); P. Unger and P. Fulde, Phys. Rev. B **48**, 16607 (1993).
- ³¹ B. Mehlig, H. Eskes, R. Hayn, and M.B.J. Meinders, (to be published).
- ³² A. Lonke, J. Math. Phys. **12**, 2422 (1971).
- ³³ S.P. Bowen, J. Math. Phys. **16**, 620 (1975).
- ³⁴ A.B. Harris and R.V. Lange, Phys. Rev. **57**, 295 (1967).
- ³⁵ G. Geipel and W. Nolting, Phys. Rev. B **38**, 2608 (1988); W. Nolting and W. Borgiel, *ibid.* **39**, 6962 (1989).
- ³⁶ D.S. Dessau *et al.*, Phys. Rev. Lett. **71**, 2781 (1993).

- ³⁷ D.M. King *et al.*, Phys. Rev. Lett. **73**, 3298 (1994).
- ³⁸ K. Gofron *et al.*, J. Phys. Chem. Solids **54**, 1193 (1993).
- ³⁹ K. Gofron *et al.*, Phys. Rev. Lett. **73**, 3302 (1994).
- ⁴⁰ R. Liu *et al.*, Phys. Rev. B **46**, 11056 (1992).
- ⁴¹ J.M. Luttinger, Phys. Rev. **119**, 1153 (1960).
- ⁴² D.M. Edwards and J. Hertz, Physica B **163**, 527 (1990).
- ⁴³ M. Luchini and D.M. Edwards, to appear in J. Low Temp. Phys.
- ⁴⁴ H. Romberg, M. Alexander, N. Nücker, P. Adelmann, and J. Fink, Phys. Rev. B **42**, 8768 (1990); C.T. Chen *et al.*, Phys. Rev. Lett. **66**, 104 (1991).
- ⁴⁵ S.L. Cooper *et al.*, Phys. Rev. B **41**, 11605 (1990); **45**, 2549 (1992); S. Uchida *et al.*, *ibid.* **43**, 7942 (1991); T. Ido *et al.*, *ibid.* **44**, 12094 (1991).
- ⁴⁶ H. Eskes and A.M. Oleś, Phys. Rev. Lett. **73**, 1279 (1994); H. Eskes, A.M. Oleś, M.B.J. Meinders, and W. Stephan, Phys. Rev. B **50**, 17980 (1994).
- ⁴⁷ A.C. Hewson and A. Wasserman, J. Phys. Cond. Matter **1**, 403 (1989).
- ⁴⁸ W. von der Linden and D.M. Edwards, J. Phys. Cond. Matter **3**, 4917 (1991).
- ⁴⁹ L.P. Gor'kov, Soviet Phys. JETP **7**, 505 (1958); Y. Nambu, Phys. Rev. **117**, 648 (1960).
- ⁵⁰ D.M. Newns, C.C. Tsuei, R.P. Huebener, P.J.M. van Bentum, P.C. Pattnaik, and C.C. Chi, Phys. Rev. Lett. **73**, 1695 (1994).

FIGURES

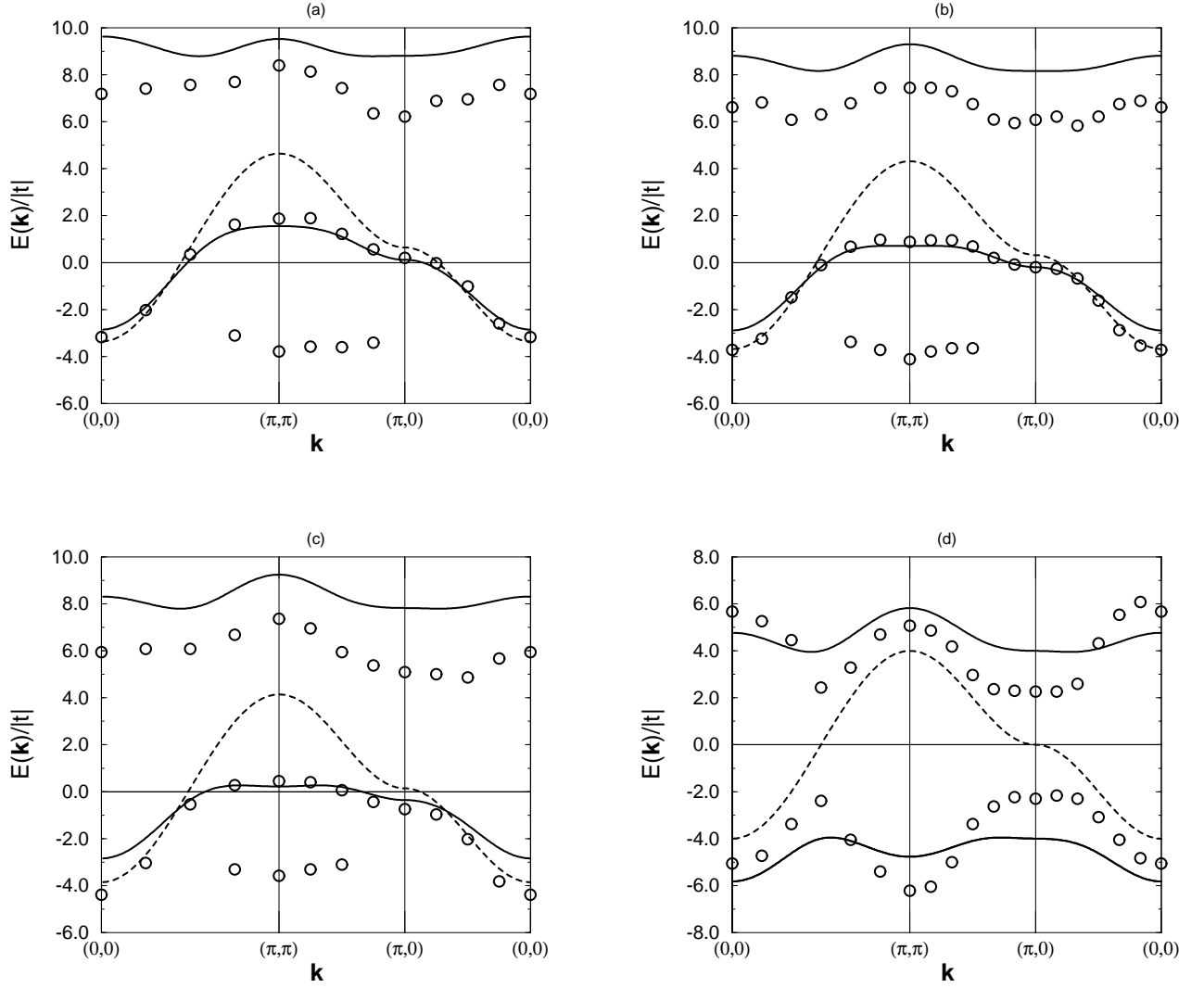


FIG. 1. The quasiparticle bands along the triangle $(0,0) - (\pi,\pi) - (\pi,0)$ for several occupations $\langle N \rangle$. The solid lines are the calculated ones for $U = 8|t|$; the circles are the results from the Quantum Monte Carlo calculations by Bulut *et al.*²⁴ for the same parameters. The dashed line indicates the band in the noninteracting ($U = 0$) case for the given occupation. (a) $\langle N \rangle = 0.75$; (b) $\langle N \rangle = 0.87$; (c) $\langle N \rangle = 0.94$; and (d) $\langle N \rangle = 1.0$ (half-filling).

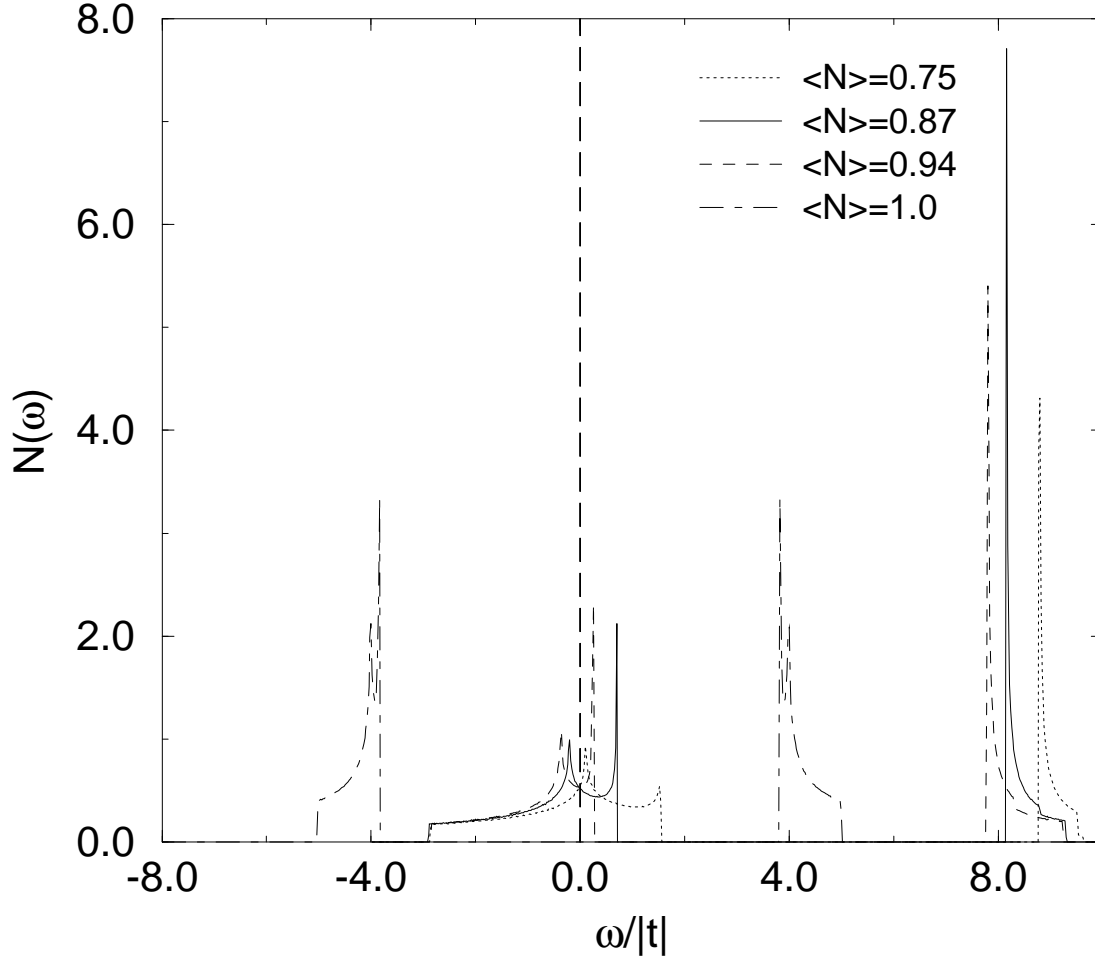


FIG. 2. The density of states for $U = 8|t|$ and the occupations as in figure 1(a)-(d).

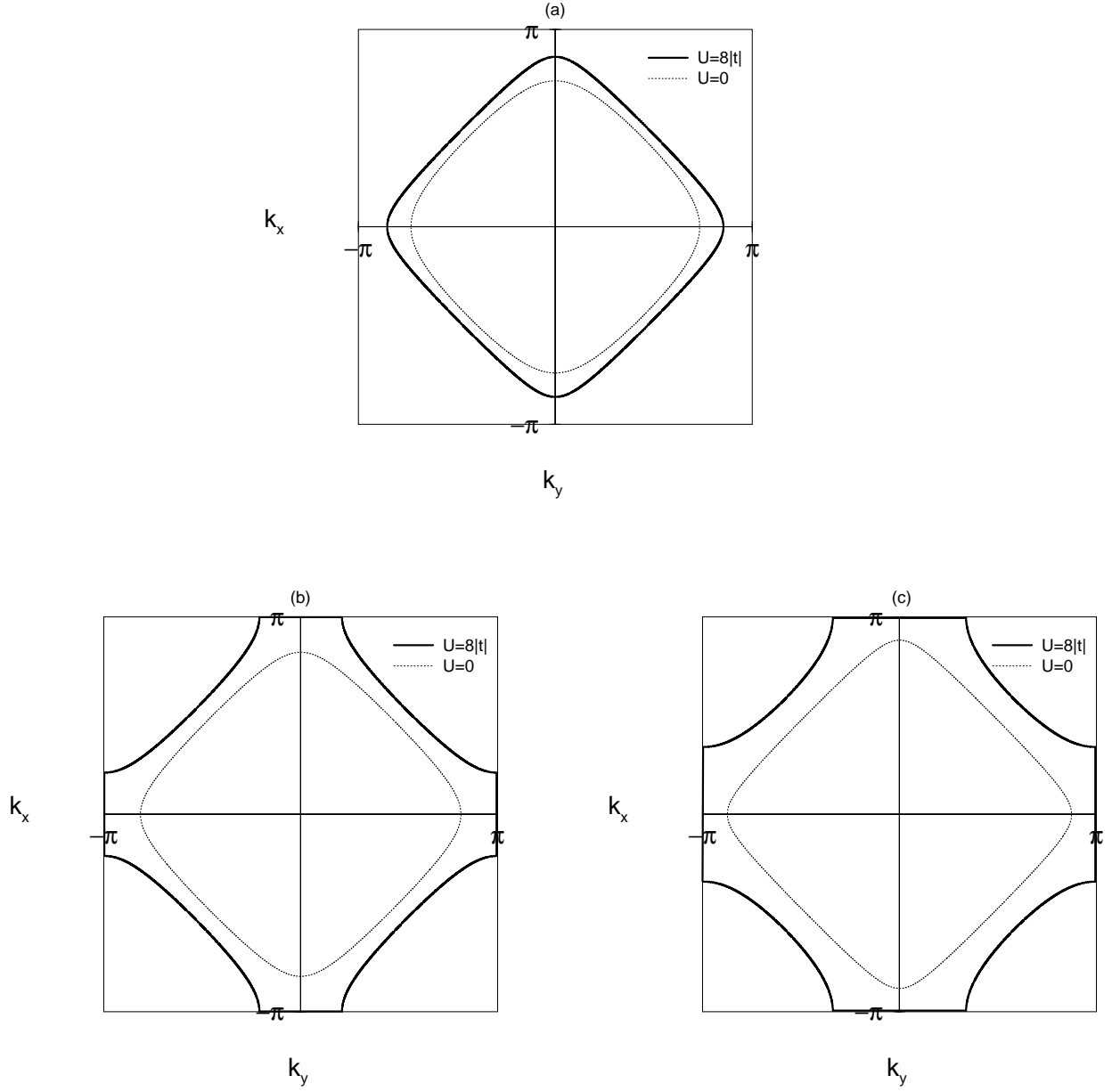


FIG. 3. The Fermi surface for $U = 8|t|$ and the occupations as in figure 1(a)-(c). For comparison the Fermi surfaces for the same occupations in the non-interacting case ($U = 0$) are shown (dotted lines).

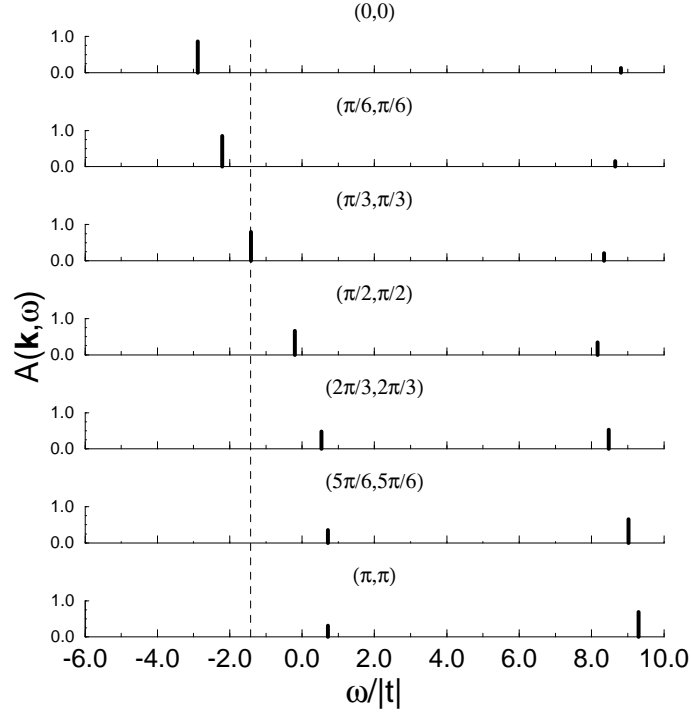


FIG. 4. The single particle spectral weight $A(\vec{k}, E)$, along the $k_x = k_y$ line, from our calculations. The height of the bars represents the weight of the delta functions. The weights of the delta functions compare well with the area's under the peaks of Fig. 1(c) in Bulut *et.al.*, Phys. Rev. B **50**, 7215 (1994). ($\langle N \rangle = 0.87$; $U = 8|t|$)

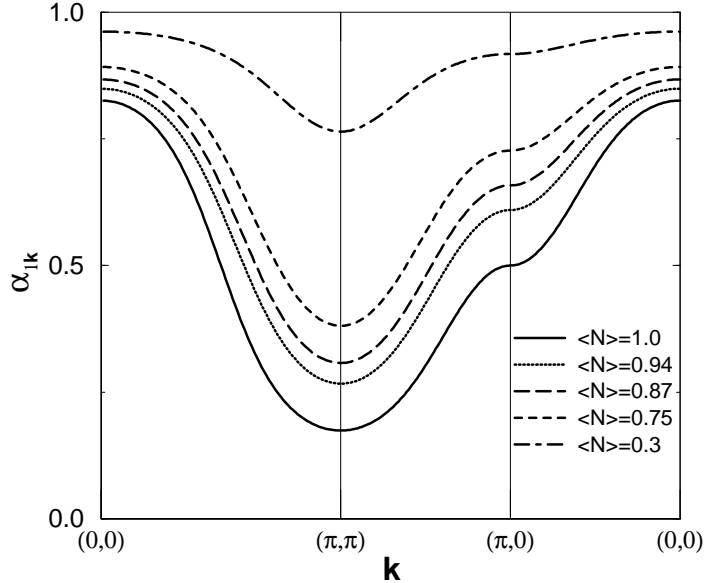


FIG. 5. The spectral weight $\alpha_{1\vec{k}}$ of the lower band for several occupations $\langle N \rangle$. Note that the sum of the spectral weights of the two bands is 1, so that this figure shows a weight transfer from the upper to the lower band upon doping. ($U = 8|t|$)

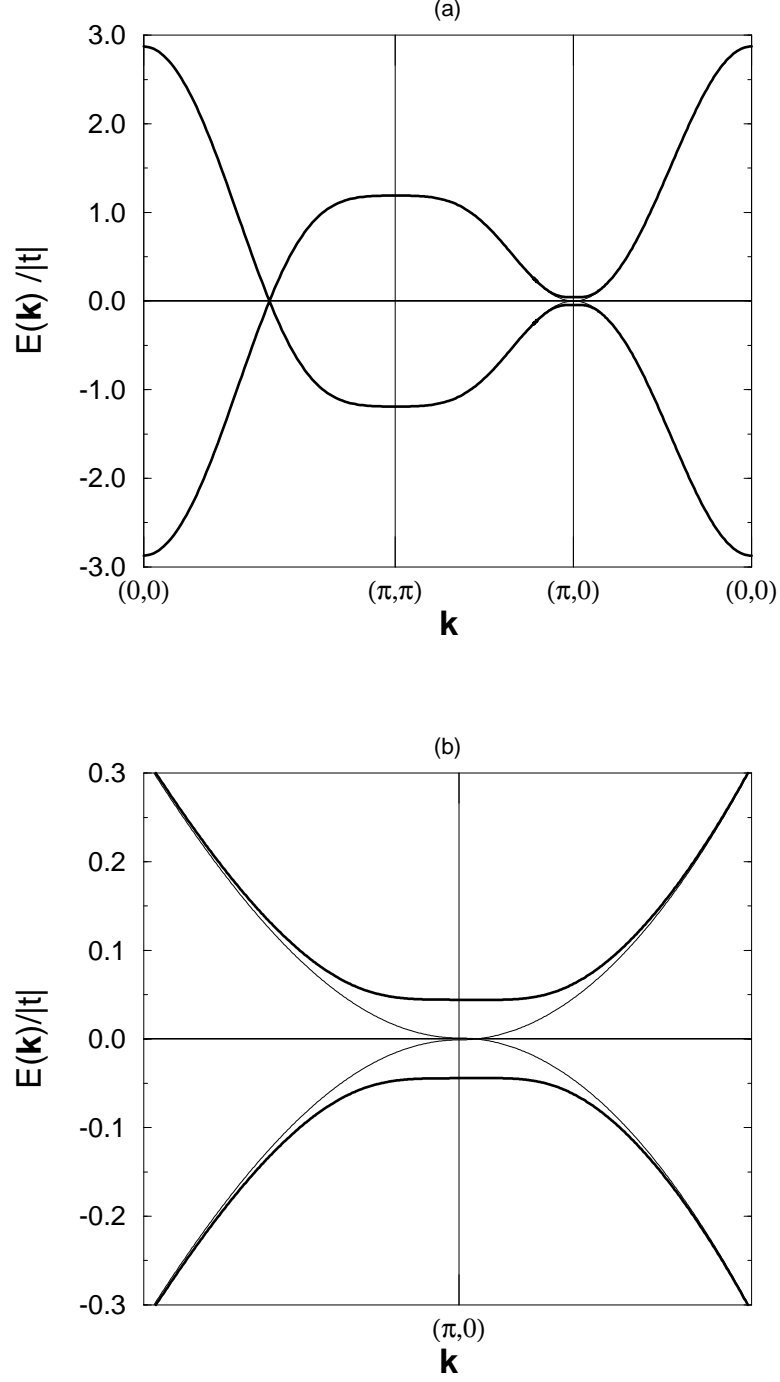


FIG. 6. (a) The 2 bands close to the Fermi surface in the superconducting state, calculated using the factorization procedure. Note the gap in the neighbourhood of the $(\pi,0)$ point and the zero gap on the $k_x = k_y$ diagonal, reflecting the d -wave symmetry. Here $U = 8|t|$ and $\langle N \rangle = 0.795$ (nearly optimum doping). (b) shows the neighbourhood of the $(\pi,0)$ -point in detail. The normal state electron and hole bands are shown in thin lines.

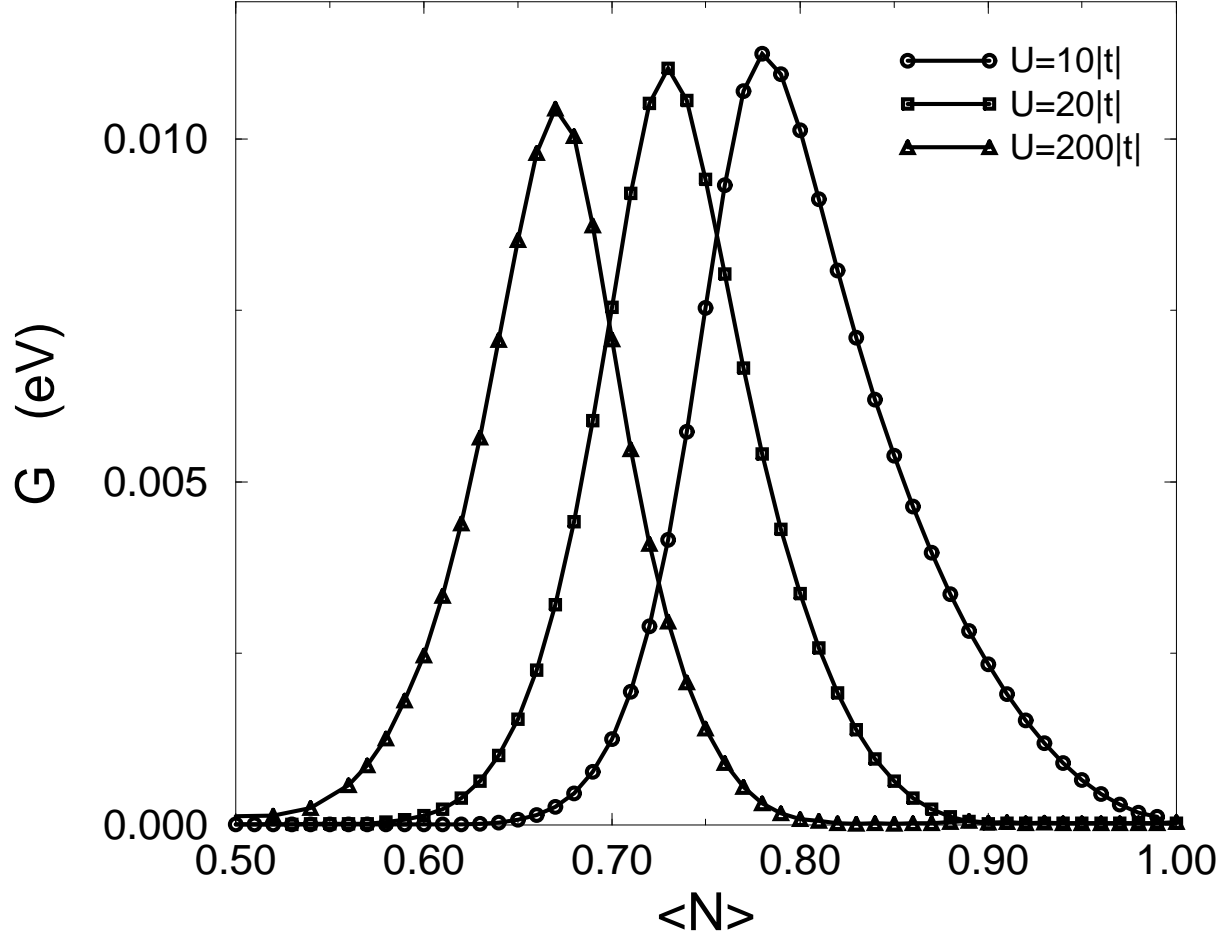
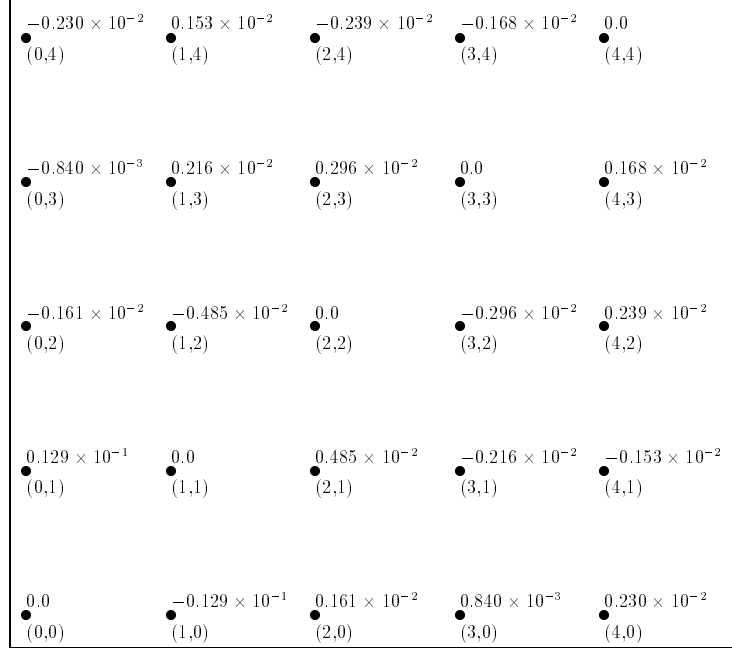
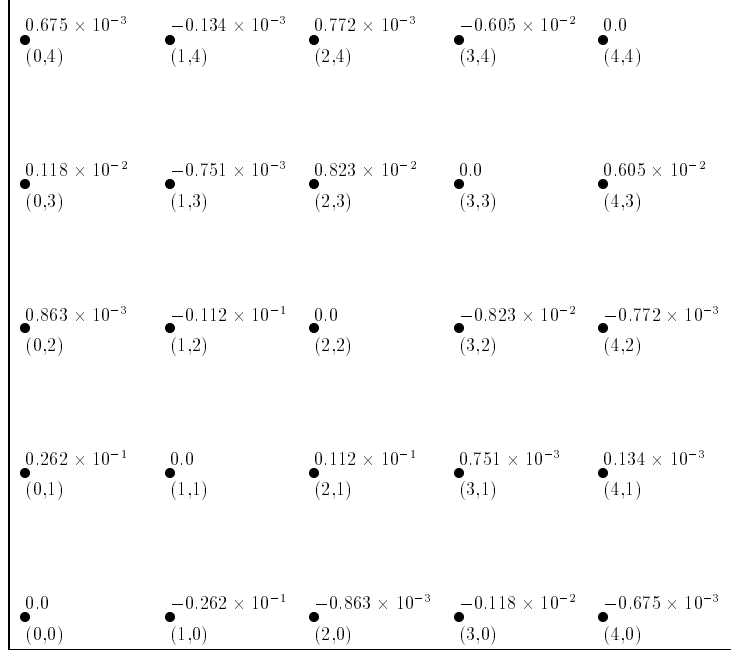


FIG. 7. The gap amplitude G as a function of the occupation $\langle N \rangle$ for several ratio's $U/|t|$, calculated using the factorization procedure. ($|t| = 0.5\text{eV}$).

(a)



(b)



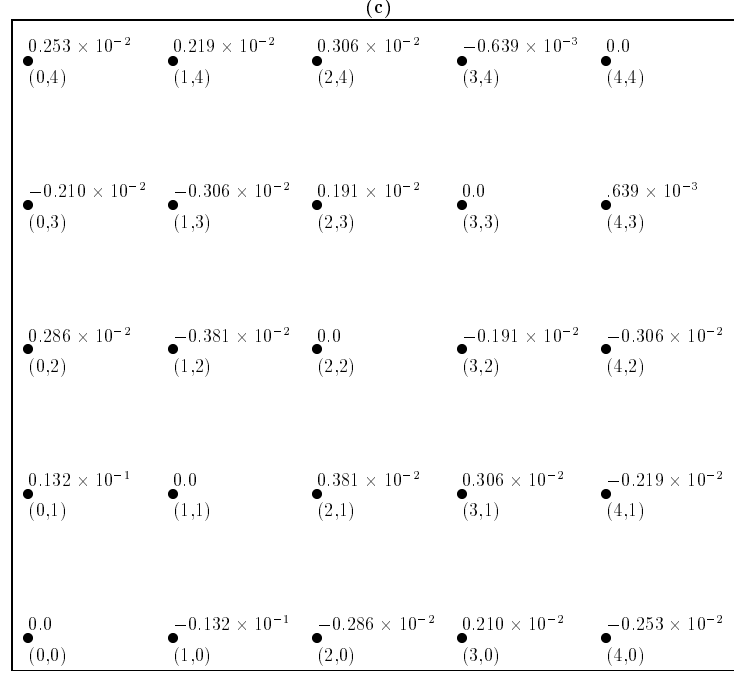


FIG. 8. Values of the pair wave function $\langle c_{i-\sigma} c_{l\sigma} \rangle$ for several lattice vectors $\vec{R}_i - \vec{R}_l$. The pair wave function value is printed above the lattice points and the lattice vector is given, as a coordinate pair in units of the lattice constant, below the lattice points. $U = 12|t|$. (a) $\langle N \rangle = 0.72$ (overdoping), (b) $\langle N \rangle = 0.76$ (optimum doping), and (c) $\langle N \rangle = 0.82$ (underdoping).

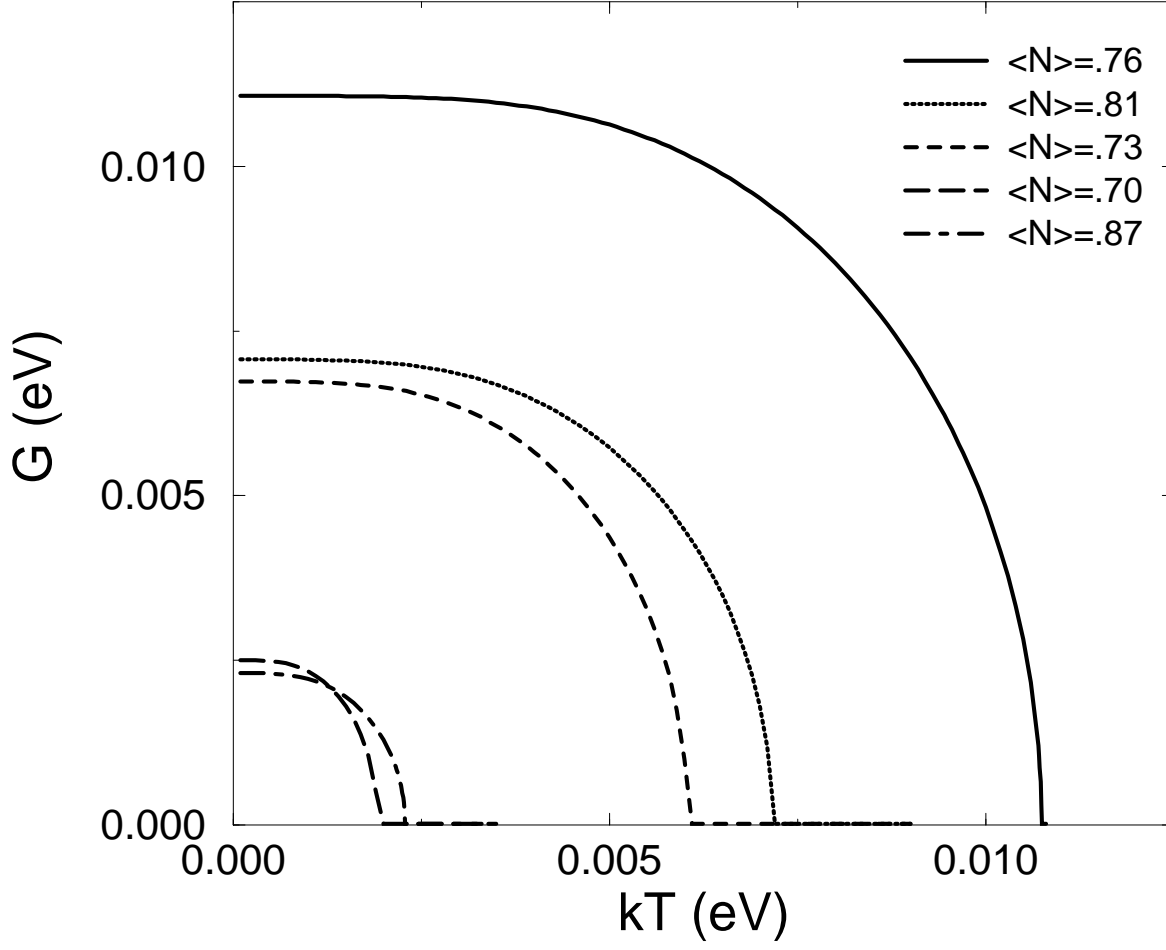


FIG. 9. The gap amplitude G as a function of temperature for $U = 12|t| = 6\text{eV}$ for several occupations $\langle N \rangle$, calculated using the factorization procedure. Note that the maximum gap $\Delta = 4G$ at optimum doping δ_c ($=0.24$ here).

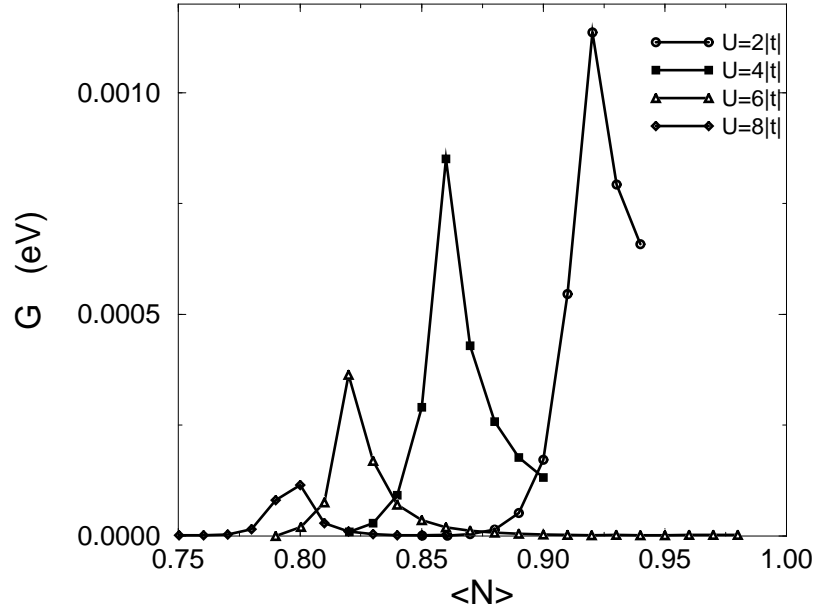


FIG. 10. The gap amplitude G as a function of the occupation $\langle N \rangle$ for several ratio's $U/|t|$, calculated using a decoupling of the gap-function that is correct in the limit $U \rightarrow \infty$. ($|t| = 0.5eV$).

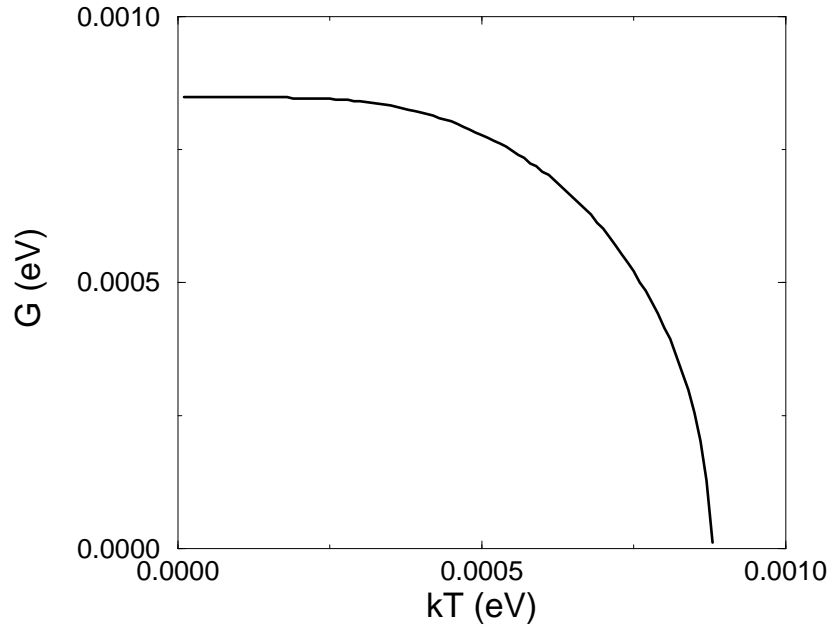


FIG. 11. The gap amplitude G as a function of temperature for $U = 4|t| = 2eV$ for optimum doping $\delta_c = 0.14$, calculated using a decoupling of the gap function that is correct in the limit $U \rightarrow \infty$.